IEEE Access
Multidisciplinary ⋮ Rapid Review ⋮ Open Access Journal

Received 26 June 2023, accepted 21 July 2023, date of publication 25 July 2023, date of current version 2 August 2023.

Digital Object Identifier 10.1109/ACCESS.2023.3298570

RESEARCH ARTICLE

Parameter Identification of Heavy-Duty Manipulator Using Stochastic Gradient Hamilton Monte Carlo Method

QI WANG[1,2,3], HUAPENG WU[2], YUNTAO SONG[1,2], HEIKKI HANDROOS[2], (Member, IEEE), YONG CHENG[1,2], AND GUODONG QIN[1,2]

[1]Institute of Plasma Physics, Hefei 230031, China
[2]Hefei Institutes of Physical Science, Chinese Academy of Sciences, Hefei 230031, China
[3]School of Energy Systems, Lappeenranta University of Technology, 53851 Lappeenranta, Finland

Corresponding authors: Qi Wang (qi.q.wang@lut.fi) and Huapeng Wu (huapeng.wu@lut.fi)

This work was supported by the Comprehensive Research Facility for Fusion Technology Program of China under Contract 2018-000052-73-01-001228.

ABSTRACT This study focuses on the parameter identification of a heavy-duty manipulator used in the remote maintenance of the China Fusion Engineering Test Reactor (CFETR). Accurate modeling of the manipulator's dynamics needs investigation of the effects of hysteresis, velocity, and other variables on output torque independently. For this reason, we estimate the undetermined model parameters using the Stochastic Gradient Hamiltonian Monte Carlo (SGHMC) method. In addition, a global sensitivity analysis is performed to assess the precision of the model's output and the relative significance of its input variables. Experiments are conducted to determine the output torque, hysteresis displacement and velocity of the CFETR's heavy-duty manipulator. Our findings indicate that the SGHMC method significantly improves the efficacy of parameter identification while maintaining a high level of accuracy, resulting in a significant reduction of approximately 8% in the root mean square error (RMSE) of the output torque. In addition, the analysis of first-order and total-effect sensitivity indices reveals the influential parameters on the output torque. The sensitivity analysis offers valuable insights into the significance of parameters and system optimization. Considering hysteresis deformation, this study presents a method for modeling and parameter estimation of the output torque in a heavy-duty robotic arm. The developed method contributes to the solution of practical problems and provides the groundwork for future research on SGHMC and parameter estimation algorithms.

INDEX TERMS Hysteresis, HMC method, parameter estimation.

I. INTRODUCTION

In recent years, the estimation of model parameters has garnered a growing amount of interest across a variety of disciplines. Academics have paid close heed to previous work on modeling the output torque of a robotic arm. The two most influential factors of output torque are friction and stiffness. The approaches to modeling the output torque can be categorized into two broad categories: model-based and model-free. Lagrangian and Newton-Euler methods [1] are included in the model-based approach. However, the specific traditional equations that assume a fixed matrix of joint stiffness are not appropriate for modeling flexible robotic arms accurately [2]. These equations oversimplify the system's behavior by neglecting the variations in stiffness that can occur with changes in load and speed. These models are inadequate for accurately reproducing modern industrial manipulators because it does not account for the elasticity of the links and bearings in the manipulator. These additional sources of elasticity have the potential to significantly impact the manipulator's behavior, necessitating a more inclusive model to accurately describe its dynamics. Consequently, there are numerous models for calculating the output torque of a flexible joint, taking into account the

The associate editor coordinating the review of this manuscript and approving it for publication was Wentao Fan.

This work is licensed under a Creative Commons Attribution-NonCommercial-NoDerivatives 4.0 License.
For more information, see https://creativecommons.org/licenses/by-nc-nd/4.0/

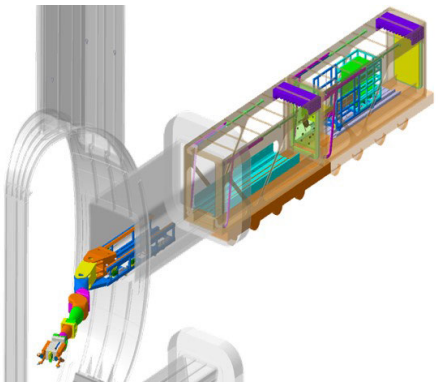

FIGURE 1. Simulation Diagram of Multifunctional Heavy Duty Maintenance Manipulator Working Scene in China Fusion Engineering Test Reactor (CFETR).

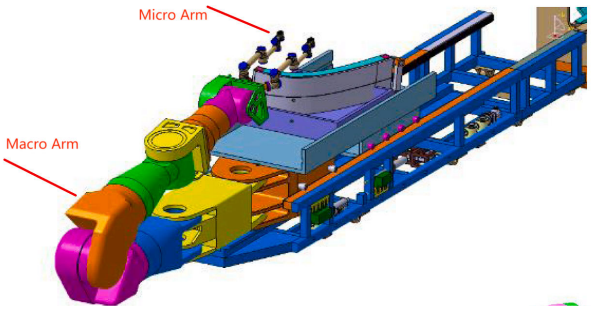

FIGURE 2. Structure of CMOR of the heavy-duty manipulator.

stiffness [3], [4] of the joint. The most recent model-based methods employ analytical models, data-driven models [5], [6], etc. Model-free approaches consist of neural network-based approaches [7], reinforcement Learning methods [8], Adaptive Control methods [9], etc. In the context of heavy-duty applications, modeling flexible robotic arms equipped with planetary gear reducers is the subject of a few articles. While there are numerous studies on the flexibility of robotic arms with harmonic reducers [10], [11], [12], there is a lack of research on the flexibility of robotic arms with planetary gear reducers under high loads. Recent research has obtained precise heavy-duty arm control through deformation modeling [13], [14]. However, a limitation of these studies is that the online precision control algorithm relies on a limited number of positions for deformation calculation. This may result in potential inaccuracies in estimating the CMOR's deformation at other positions. Considering the limitation in the study on deformation, further parameter identification of the heavy-duty manipulator is crucial. By employing the stochastic gradient Hamilton Monte Carlo method, our research aims to enhance the understanding and estimation of parameters related to the overload arm, filling the existing gap in knowledge, and improving the overall performance and precision control of the manipulator under heavy loads.

The goal of this paper is to extend the original model of the dynamics equation of a single joint mechanism in section II-A by using the Stochastic gradient Hamilton Monte Carlo [15] (SGHMC) method to include (a) hysteresis effects and (b) a more appropriate posterior parameter distribution on hysteresis effects to predict the output torque with high-frequency oscillations. Extending a Bayesian model and estimating the output torque of a heavy load manipulator constitute the final phase.

The CFETR Multipurpose Overload Robot (CMOR) is a heavy-duty manipulator designed for remote maintenance tasks in the China Fusion Engineering Test Reactor (CFETR), as depicted in Figure 1 and Figure 2. The CMOR is a flexible and heavy-duty fusion robot designed with a multi-degrees-of-freedom macro and micro mechanical structure, enabling it to operate in a large working space under vacuum conditions. The macro arm of the CMOR consists of a 9-degrees-of-freedom Multi-Purpose Deployer (MPD) robot [16], while the micro arm comprises a dual 7-degrees-of-freedom robot. Figure 2 illustrates the configuration of the CMOR system [17]. Figure 3 showcases the experimental platform for the fourth joint of the MPD.

The CMOR robot arm, integrated within the CFETR superconducting Tokamak fusion device, serves as a teleoperation and maintenance robot arm with nine degrees of freedom and a mass exceeding 25 tons. Under the 9-degrees-of-freedom mode, the maximum designed load capacity is two tons. The structure of CMOR, as shown in Figure 1, imposes a significant burden on each joint. Consequently, the motor driving the joints must possess a high reduction ratio. The J4 joint, for instance, exhibits a maximum output torque of 100 KN · m with a total reduction ratio of 11000. However, the high load and large reduction ratio can lead to decreased torque transmission efficacy, subsequently affecting the manipulator's control precision.

The following are descriptions of several essential components:

- Base: The base provides support and securement for test components and equipment.
- Loading shaft: The loading shaft transmits the shear force, bending moment, and torque exerted by the hydraulic cylinder onto the test joint.
- Hydraulic system: The hydraulic system employs a Y-type reversing valve with a hydraulic lock and an accumulator to maintain pressure. The hydraulic cylinder centering mechanism prevents deformation of the bearing seat in any direction other than vertical.
- Dynamometer: The dynamometer actively loads the test joints and typically consists of a reducer, servo motor, etc.

For detailed technical design and joint loading force indicators, please refer to Appendix B.

The overall configuration of the CMOR heavy-duty manipulator is as follows: The mechanical arm body structure design requires dimensions of Width × Height $\leqslant$ 2740 mm × 2330 mm. The J4 joint has a maximum load capacity of 120 KN · m. The manipulator's specifications include a repetitive positioning accuracy of $\pm$10 mm, and a maximum

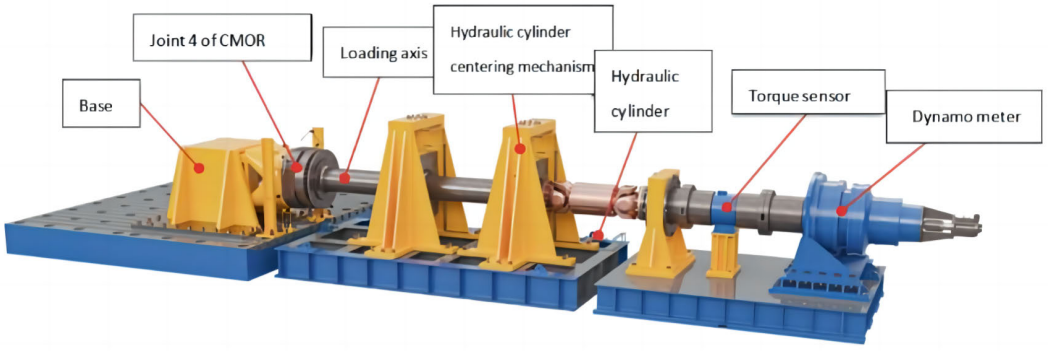

FIGURE 3. CMOR single-joint experimental platform (The 4th joint).

TABLE 1. Joint type and range.

Joint	Type	Range
Joint 1	Move	$0-6000$ mm
Joint 2	Yaw	$\pm 90°$
Joint 3	Yaw	$\pm 90°$
Joint 4	Roll	$\pm 180°$
Joint 5	Pitch	$0-180°$
Joint 6	Roll	$\pm 180°$
Joint 7	Pitch	$\pm 90°$
Joint 8	Roll	$\pm 130°$
Joint 9	Pitch	$\pm 90°$

operating speed of 100 mm/s. The types and ranges of the joints are presented in Table 1.

Taking the J4 joint as an example, it is driven by three motors in the driving part. This configuration ensures that if one of the three motors fails, the remaining two motors can continue driving the J4 joint to facilitate subsequent maintenance. In the transmission part, a precision reducer and differential planetary gear transmission are employed to meet the requirements of high load and a high reduction ratio from the motor output end to the joint output end. However, the complex structure of the transmission system poses challenges in joint modeling, resulting in a large equivalent rotor moment of inertia and increased non-linearity at the motor end.

To enhance the understanding of the system's operation, a control system diagram has been included in Appendix C. This visual representation provides a clear overview of the components and interactions involved in the control process. Additionally, comprehensive details regarding the measuring techniques have been provided. This includes information on the types of sensors used and the calibration procedures employed to ensure accurate data acquisition for parameter estimation.

In the process of dynamic parameter identification, it is typically necessary to estimate the model parameters, such as by employing the least squares or maximum likelihood estimation techniques to acquire the point estimation value of the model parameters. However, the uncertainty of model parameters is not reflected in this point estimate. By using Bayesian methods, it is possible to derive a posterior distribution of model parameters, which provides more complete information, including optimal estimates and uncertainty information. The posterior probability distribution is usually complex and contains integrals that cannot be solved directly. The application of the MCMC (Markov chain Monte Carlo) algorithm [18] gives new vitality to the Bayesian method, and of course, it cannot be separated from the great improvement of computer computing power. MCMC includes two MCS. The first one is the Markov chain, which is used to solve the problem of sampling from arbitrary probability density (usually refers to those probability density functions that cannot directly obtain the cumulative distribution function (CDF)); The second is Monte Carlo, which is used to solve the complex integral solution. Metropolis–Hastings (MH) algorithm has been highly praised in various sampling-related fields since it first appeared in the 1950s, such as economics [19], astronomy [20], psychology [21], and so on. There are two main reasons: 1. MH algorithm steps are very simple, see Section II-B; 2. MH algorithm can sample from complex target distribution, regardless of the specific form of the target distribution.

Later developed Hamiltonian Monte Carlo (HMC) [22], slice sampling[4], elliptical slice sampling (ESS) [23], generalized elliptical slice sampling(GESS) [24], Langevin Monte Carlo [25], stochastic gradient Langevin dynamic [26], and so on can be regarded as one kind of MH.

During the actual application of MCMC, the following problems may be encountered, such as 1. The transition kernel of MH may cause random walk behavior, which may cause the effective sample size (ESS, which measures the number of valid or unrelated samples) to be small and the sampling efficiency to be too low; 2. Also, when the objective function is multi-modal, all modes cannot be found.

3. The rejection rate of the MH algorithm is related to the transition kernel. We hope that the rejection rate is as low as possible.

The Hamiltonian Monte Carlo (HMC) algorithm proposed later is famous for its ability to solve the above problems. Compared with the MCMC algorithm, HMC (Hamiltonian Monte Carlo) is a faster sampling method. Recently, many modifications have been made to the HMC method in computational statistics to form a new algorithm [27].

In Hamilton Monte Carlo, one is Hamilton and the other is Monte Carlo. Among them, Hamilton here comes from dynamics and corresponds to Hamiltonian dynamics, which is often used to describe the motion process of objects. See section II-B for details of the SGHMC algorithm.

In summary, the Stochastic Gradient Hamiltonian Monte Carlo (SGHMC) is a variation of the technique Markov Chain Monte Carlo (MCMC) that is used to sample from complex probability distributions. SGHMC uses stochastic gradient descent (SGD) to execute the sampling, allowing for faster convergence and improved scalability with bigger datasets. Here are some benefits of SGHMC versus MCMC:

1. With conventional MCMC, convergence can be slow, particularly for high-dimensional models or big data sets. SGHMC makes advantage of SGD, which modifies the parameters more frequently and in smaller increments, resulting in speedier convergence.

2. Improved scalability: As the amount of the dataset grows, MCMC techniques can become computationally costly. SGHMC is more scalable since it changes parameters in mini-batches, enabling it to efficiently manage larger datasets.

3. SGHMC is more robust than regular MCMC to noise in the data. Because it changes the parameters using a stochastic gradient, it can deal with noisy data without becoming stuck in local minima.

4. Automatically adapts step size: In conventional MCMC, it might be difficult to choose an acceptable step size for the updates, particularly in high-dimensional domains. SGHMC makes it easier to use by automatically adjusting the step size based on the gradient and noise level of the data.

5. In MCMC, evaluating the gradient of the log-likelihood function can be computationally demanding, particularly in high-dimensional models. SGHMC simply requires an unbiased estimate of the gradient, which can be computed more quickly and with less effort.

The low transmission efficacy of a heavy-duty manipulator is primarily attributable to the heavy friction force of a heavy-duty manipulator in comparison to a light-duty manipulator. It is now well established that friction [28], [29] and hysteresis effects [30] can impair torque transmission efficiency. Until now no experiments on the single joint of heavy-duty manipulator equipped with differential planetary gears have been reported.

Since this article only mentions a single joint, several clarifications are necessary. After modeling, the following was determined:

a. The dynamic model is based on Lagrange, the parameters of each connecting rod of the robot consist of 10 items and are directly related to the torque, and the torque is proportional to the product of the dynamic parameters.

b. The dynamic properties model for each connecting rod, which is based on Lagrange, consists of identifiable components (seven items) and undetermined components (three items).

c. When the moment of inertia of the motor's rotor appears in the dynamic equation of the torque equation for each motor, the connecting rod and its matching motor of the subsequent joint are typically considered a unit. Based on the LaGrange equation, it can be determined that: the rotor of the motor (a portion of the stator is assumed to be part of the connecting rod) in the dynamic equation, as the rotor rotation (I_m), is typically very small in comparison to the mass of the robotic arm, we only consider $I_m \times n^2$, where n is the corresponding reduction ratio. Since there is only one joint in this article, there is no $I_m \times n^2$. If two or more joints exist, the parameter $I_m \times n^2$ must be added. As previously stated, the connecting rod of the preceding robotic arm and the rotor of the following robotic arm is regarded as a unit.

d. Friction utilizes the classical model, which incorporates viscous friction and Coulomb friction (a more comprehensive analysis will be provided in the following paper).

e. Once the joints of the heavy-duty robotic arm have been connected, the complete dynamic equation can be found by adding $I_m \times n^2$ to the Lagrange or classical Bouc-Wen model introduced in the second section, which can identify all identifiable dynamic components. This article has limited conditions and only one joint data, so only parameters without $I_m \times n^2$ are used to determine the output torque.

This paper first introduces the MCMC algorithm which uses the MH method to sample and the SGHMC algorithm. Secondly, the SGHMC method was used to identify the parameters of the classical Lagrange dynamic modeling of a robot manipulator [1] and the CBW (the classical Bouc-Wen) model [31], [32], [33], the accuracy of the two models was compared, and the hysteresis model parameters were identified. Finally, the global sensitivity of the CBW model and hysteresis formula is analyzed.

II. THE DYNAMIC MODEL

A. THE CLASSICAL LAGRANGE DYNAMIC MODELING AND THE CLASSICAL BOUC-WEN MODEL (CBW) OF A ROBOT MANIPULATOR

The dynamic characteristics of the manipulator consist mostly of position parameters, such as the angle, angular velocity, and angular acceleration of each joint, which can be determined through encoder measurement and differential processing. It is simple to gather structural parameters, such as the length of each connecting rod on the robot, by measurement. Inertial characteristics, such as the mass of the connecting rod, the moment of inertia, and the location of the center of mass, are the primary elements influencing

TABLE 2. Standard DH (SDH) parameter of the fourth joint of CMOR.

a/rad	a/mm	d/mm	θ/rad
$\pi/2$	0	0	$\theta 1$

the robot's dynamic model. The parameters differ from the design parameters. If the design parameters are imported directly into the dynamic model, a significant variation will occur. The direct measuring method, such as disassembling the mechanical arm and weighing the process, is excessively complex and unsuitable for use in actual situations. Friction parameters, for non-directly driven articulated manipulators, the torque to overcome friction accounts for approximately 25 % of the driving torque, the structure of the drive system, the contact type between components, the lubrication conditions of the contact surface, and the relative movement speed of the contact surface, load, etc. all influence friction.

1) MODEL THE ROBOT'S DYNAMICS BASED ON LAGRANGE

As shown in equation (4) the dynamics equation of a single joint mechanism, Table 2 is the Standard Denavit-Hartenberg parameters(SDH) parameter of the fourth joint of CMOR [17], [34]. The joint output torque consists of inertia torque, centrifugal force torque, Coriolis force torque, gravity torque, and friction torque. The procedure of identifying parameters entails determining the real mass attribute of the joint, the real moment of inertia, and the viscous and Coulomb friction coefficients, respectively.

The robot dynamics model in (1) can be written in the linear form of its moment of inertia parameters without considering friction and presuming that all connecting rods are rigid bodies (regardless of the flexibility of the connecting rods).

$$Y(q, \dot{q}, \ddot{q})P = \tau \tag{1}$$

where P is the complete inertial parameter set (standard parameters), which includes the unknown parameters of the robot model that need to be estimated or identified. These parameters can include the inertial parameters of the robot links (such as mass, center of mass, and inertia tensor components), friction parameters, and other parameters that affect the robot's dynamics. $Y(q, \dot{q}, \ddot{q})$ represents the dynamic matrix, which describes the relationship between the joint positions q, joint velocities $\dot{q}$, and joint accelerations $\ddot{q}$. It captures the dynamic behavior of the system and is typically derived from the robot's equations of motion.

τ represents the joint torque vector, which represents the torques or forces applied to the robot's joints. These torques can be generated by various factors, such as external loads, actuator dynamics, and control inputs. By solving this equation, we can estimate the unknown parameters of the robot model based on the measured joint torques and kinematic information.

$$P_i = \left[I_{ixx}, I_{ixy}, I_{ixz}, I_{iyy}, I_{iyz}, I_{izz}, m_i r_x, m_i r_y, m_i r_z, m_i\right]^T \tag{2}$$

In Equation (2), the vector P_i represents the parameters associated with the i-th link of a robot manipulator. The meaning of each parameter is explained below:

I_{ixx} is the moment of inertia of the i-th link around the x-axis. I_{ixy} is the product of inertia of the i-th link between the x and y axes. I_{ixz} is the product of inertia of the i-th link between the x and z axes. I_{iyy} is the moment of inertia of the i-th link around the y-axis. I_{iyz} is the product of inertia of the i-th link between the y and z axes. I_{izz} is the moment of inertia of the i-th link around the z-axis. r_x is the distance from the center of mass of the i-th link to the x-axis. r_y is the distance from the center of mass of the i-th link to the y-axis. r_z is the distance from the center of mass of the i-th link to the z-axis. m_i is the total mass of the i-th link.

The Coulomb and viscous friction models are:

$$\tau_f = [f_v, f_c]\begin{bmatrix} \dot{q} \\ \mathrm{sgn}(\dot{q}) \end{bmatrix} \tag{3}$$

In Equation (3), the vector τ_f represents the friction torque applied to the robot joints. Let's explain the meaning of each parameter:

f_v is the viscous friction coefficient. It represents the damping effect in the joint motion, where the magnitude of the friction torque is proportional to the velocity of the joint $\dot{q}$. f_c is the coulomb friction coefficient. It represents the static friction or stiction in the joint motion, where the friction torque remains constant until a threshold velocity is reached. The sign function $\mathrm{sgn}(\dot{q})$ is used to determine the direction of the Coulomb friction torque. This friction torque affects the dynamics of the manipulator and needs to be considered for accurate modeling and control of the robot's motion.

Consider the torque effect of friction at the joints. As a result, the following (4) exist:

$$\begin{aligned} \tau &= Y'p' \\ &= [\ddot{q}, 0, 0, 0, 0, 0, g\sin(q), g\cos(q), 0, 0, \dot{q}, \mathrm{sgn}(\dot{q})] \\ &\quad \cdot \left[I_{xx}, I_{xy}, I_{xz}, I_{yy}, I_{yz}, I_{zz}, m\,r_x, m\,r_y, m\,r_z, m, f_v, f_c\right]^T \end{aligned} \tag{4}$$

In Equation (4), the vector τ represents the total torque exerted on the robot joints. The meaning of each parameter is explained below:

$\ddot{q}$ is the joint acceleration vector. g is the acceleration due to gravity. q is the joint angle vector. It represents the current positions of the robot joints. I_{xx}, I_{xy}, I_{xz}, I_{yy}, I_{yz}, I_{zz} are the elements of the inertia matrix. These parameters represent the moments of inertia of the robot's links around different axes. m is the link mass. r_x, r_y, r_z are the link center of mass position. These parameters represent the distances between the joint axis and the center of mass of the links along different axes. f_v is the viscous friction coefficient. It represents the damping effect in the joint motion. f_c is the coulomb friction coefficient. It represents the static friction or stiction in the joint motion. The equation computes the total torque τ experienced by the robot joints. This torque accounts for the effect of joint acceleration, gravity, inertia, mass distribution, and friction in the robot's dynamics.

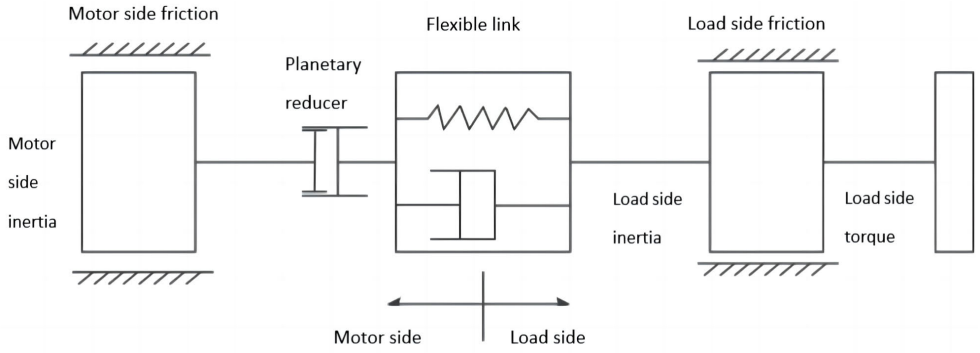

FIGURE 4. Flexible joint structure diagram.

2) THE CLASSICAL BOUC-WEN MODEL (CBW)

The preceding formula considers the joint to be a rigid material. If the formula for identifying the parameters of a flexible joint is used, the stiffness coefficient and damping coefficient must be identified. Below Figure 4 is a schematic representation of a flexible joint's structure.

The identification (5) of the traditional flexible joint parameter identification is as follows [35],

$$\tau(\phi, \dot{\phi}) = K_s(\theta/\eta - q) + K_d(\dot{\theta}/\eta - \dot{q}) \tag{5}$$

where $q, \theta, \dot{q}, \dot{\theta}$ are the torsional angle and torsional angular velocity between the motor side and the load side, respectively. η is the joint reduction ratio, k_s is the stiffness of the joint system, k_d is the damping coefficient of the flexible link.

Shown in Figure 5, the Bouc-Wen model [36] is shown in the three equations below.

Our objective is to accurately measure the angular displacement, or joint torsion, between the input and output of the joint. Joint torsion, denoted as $\Delta\theta(t)$, represents the positional deviation or difference between the desired input and the actual output of the joint.

The equation governing joint torsion is expressed as:

$$\Delta\theta(t) = q - \frac{\theta(t)}{N} = z(t) + x(t). \tag{6}$$

In the context of our study, we do not consider backlash [30], which refers to any looseness or play in the mechanical components of the joint. Therefore, the term $x(t)$ in the hysteresis model directly represents the joint torsion as described in Equation (6). This term captures the positional deviation between the desired input and the actual output of the joint, allowing us to effectively analyze and control the elasticity of the links and bearings in the manipulator.

In one expression, the joint torque is shown as a function of the joint's position and speed. The joint's transmitted torque, T, is given by:

$$T(t) = D \times \dot{\mathrm{u}}(t) + \Gamma(\mathrm{u}(t), t) \tag{7}$$

where D is the internal damping coefficient. The following are the definitions of a Bouc-Wen-like hysteresis model:

$$\Gamma(u(t), t) = wk|u(t)| + (1 - w)k|x(t)| \tag{8}$$

where $\mathbf{u}(t)$ is the input position to the one joint system, $\dot{\mathbf{u}}(t)$ is the velocity. $\Gamma(u(t), t)$ represents the hysteresis output torque, composed of an elastic term $wk|u(t)|$ and a purely hysteretic term $(1 - w)k|x(t)|$ with the parameters k, and w. x is a hysteresis variable which is the solution of (9).

A plastic torque response (w=0) and a completely elastic torque response (w=1) are weighted differently. Stiffness is denoted by k. The nonlinear hysteresis x of the Bouc-Wen model is determined by the following differential (9):

$$\dot{x}(t) = \alpha\dot{\mathrm{u}}(t) - \beta|\dot{\mathrm{u}}(t)\|x(t)|^{n-1}x(t) - \gamma\dot{\mathrm{u}}(t)|x(t)|^n \tag{9}$$

The friction term is:

$$f = f_c \times \dot{u}(t) + f_v \times \mathrm{sgn}(\dot{u}(t)) \tag{10}$$

where f_c is the Coulomb friction, f_v is the viscous friction, C is the constant.

The classical Bouc-Wen (CBW) model [37] is developed to describe the hysteresis effect in (9) and the output torque in (11), we define the constants $ku = wk$, $kh = (1 - w)k$.

$$\begin{aligned} T(t) = {} & D \times \dot{\mathrm{u}}(t) + k_u \times u(t) + k_h \times x(t) \\ & + f_c \times \dot{\mathrm{u}}(t) + f_v \times \mathrm{sgn}(\dot{\mathrm{u}}(t)) + C \end{aligned} \tag{11}$$

B. EXPERIMENT WITH SETUP AND IMPLEMENT

1) EXCITATION OF FOURIER SERIES TRAJECTORY

The input of the dynamic equation is the robot's position and current during operation, which are determined by designing a robot's motion trajectory. a. Each joint's Fourier series has 2*N+1 parameters. This experiment uses the method of combined connecting rods to determine the dynamic properties of each combined body's individually identifiable sections. b. Regarding the selection of excitation frequency, it should be mentioned that selecting a low frequency has the following benefits: Under the maximum acceleration, speed, and displacement limits, it is possible to reach a bigger workspace, but the acquisition period is lengthy and the acceleration is low. It is not conducive to identifying parameters of inertia. High frequency has the advantages of facilitating the identification of inertia characteristics and reducing the acquisition time, but the downsides of limiting the working space and

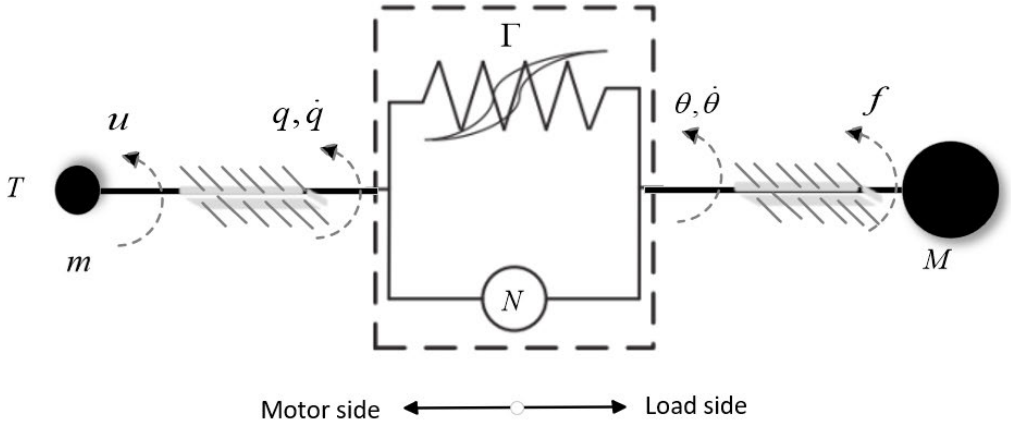

FIGURE 5. Structure of elastic robot joint.

making it simple to resonate. c. Use the smallest logarithm of the condition number of the observation matrix of the kinetic equation as the objective and optimize the Fourier series parameters [38], [39]. The position, speed, and acceleration of the excitation track are as follows (12).

$$
\begin{aligned}
q_i(t) &= \sum_{l=1}^{N_i} \frac{a_l^i}{\omega_f l} \sin\left(\omega_f l t\right) - \frac{b_l^i}{\omega_f l} \cos\left(\omega_f l t\right) + q_{i0} \\
\dot{q}_i(t) &= \sum_{l=1}^{N_i} a_l^i \cos\left(\omega_f l t\right) + b_l^i \sin\left(\omega_f l t\right) \\
\ddot{q}_i(t) &= \sum_{l=1}^{N_i} -a_k^i \omega_f l \sin\left(\omega_f l t\right) + b_l^i \omega_f l \cos\left(\omega_f l t\right)
\end{aligned} \tag{12}
$$

2) DATA COLLECTION AND EXPERIMENT PROCEDURE

To identify the above parameters, the specific steps to realize parameter identification is designed. However, since the control system can only rotate for half a turn temporarily, the excitation trajectory of the Fourier function can only rotate within the range of ±180°. It is impossible to minimize the number of conditions, and only a relatively small number of conditions can be used.

Scheme 1: measure the change of joint output torque with speed and load.

The following experiments were repeated at 300r / min and 3000r / min: start the joint motor, turn the joint angle to 0° according to the motor code disk, and set the output encoder angle to zero.

Slowly and positively load the joint output end with the dynamometer to the rated torque of 120 KN · m. Read the number of encoder pulses at the output end every 0.1 seconds. Similarly, slowly unload the bending moment at the output end from the rated torque to 0, read the pulse number of the encoder at the output end every 0.1 seconds, and convert the pulse number into an angle. At the same time, the displacement, velocity, current and other data of the joint load end are recorded.

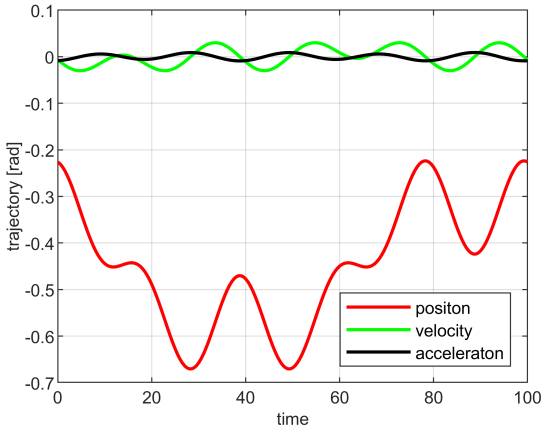

FIGURE 6. The position, speed, and acceleration of the excitation path.

Scheme 2: measurement of joint current and torque following curve.

Use the dynamometer to slowly forward load the output end of the joint, pause for 2S every 10 KN · m, load it to the maximum rated torque of 120 KN · m, record the following curve of current and torque of each motor, and record the motor temperature. Then, the above experiments were repeated at 300r / min and 3000r / min.

Scheme 3: excitation trajectory of Fourier function

The smaller the number of conditions of the optimal excitation trajectory, the better. Therefore, we use the fifth-order Fourier function, according to the position of the experimental platform. The position, speed, and acceleration of the excitation track are as follows Figure 6:

III. PARAMETER OPTIMIZATION OF THE DYNAMIC MODEL

A. THE BAYESIAN APPROACHES AND THE METROPOLIS-HASTINGS ALGORITHM

Using what we already know and data from different experiments, we can divide the ways to find parameters into

three groups: MLE (maximum likelihood estimation) [40], MAP (maximum probability estimate) [41], and the Bayesian method [15], [42].

Assuming we have training data $\mathcal{D} = \{(\mathbf{x}_1, y_1), \ldots, (\mathbf{x}_n, y_n)\}$, and parameter θ.The goal is to use new test points x' to make predictions y'. MLE does not consider prior, while MAP and Bayesian estimation considers prior. MLE and Map are to select the relatively best point estimation. The Bayesian method is to estimate the posterior distribution $p(\theta \mid \mathcal{D})$ through observation data and makes predictions $\int_\theta p\left(y' \mid x', \theta\right) p(\theta \mid \mathcal{D}) d\theta$ through the posterior distribution. Because of the nonlinear and multi-parameter characteristics of the dynamic model of the heavy-duty manipulator, the Bayesian method is a good choice.

There were other sampling methods before Metropolis-Hastings appeared. For example, rejection sampling and importance sampling [43] are independent for each sampling. In this way, each sampling cannot use the information of the previous sampling. One state of the Markov chain is only related to the previous state, so the previous sampling information is used. Assume that the objective distribution function is $\pi(x)$. In general, the Metropolis-Hastings algorithm can sample from the objective function by constructing a Markov chain converging to π. The following is the Metropolis Hasting Algorithm:

Input: Target distribution $p(\boldsymbol{\theta})$, proposal distribution $q(\boldsymbol{\theta}'|\boldsymbol{\theta})$, starting point $\boldsymbol{\theta}_0$, number of iterations N.

Output: Samples $\boldsymbol{\theta}_{1:N}$.

1) Set $t = 0$ and $\boldsymbol{\theta} = \boldsymbol{\theta}_0$.
2) For t from 1 to N repeat the following steps:
   - Sample a proposed state $\boldsymbol{\theta}' \sim q(\boldsymbol{\theta}'|\boldsymbol{\theta})$.
   - Calculate the acceptance probability: $\alpha = \min\left(1, \frac{p(\theta')q(\theta|\theta')}{p(\theta)q(\theta'|\theta)}\right)$.
   - Sample a uniform random number u from [0, 1].
   - If $u < \alpha(\boldsymbol{\theta}, \boldsymbol{\theta}')$, accept the proposal and set $\boldsymbol{\theta} = \boldsymbol{\theta}'$. Otherwise, reject the proposal and set $\boldsymbol{\theta} = \boldsymbol{\theta}$.
   - Store the current sample $\boldsymbol{\theta}$ in $\boldsymbol{\theta}_t$.
3) Output the samples $\boldsymbol{\theta}_{1:N}$.

where $p(\theta)$ is the probability density function of the target distribution, $q(\theta'|\theta)$ is the proposal distribution, and θ' and θ are the proposed and current states of the Markov chain, respectively.

B. STOCHASTIC GRADIENT HAMILTON MONTE CARLO (SGHMC)

The cornerstone of HMC [44] is the following Hamiltonian dynamic [45]. By introducing Hamiltonian dynamics, the SGHMC algorithm can perform efficient Bayesian inference on large-scale datasets.

HMC algorithm should also be regarded as a Metropolis Hasting algorithm, which realizes the initial state transition through the Hamiltonian partial differential equation and satisfies the detailed and stable conditions through the acceptance-rejection algorithm. The difference from the ordinary Metropolis Hasting algorithm is that its initial state transition is determined, that is, the probability is 1 (compared with the ordinary random walk method, the acceptance probability is increased, and the convergence speed is improved).

Hamiltonian system in (13) and (14):

$$H(q, p) = U(q) + K(p) \tag{13}$$

$$\frac{\partial q_i}{\partial t} = \frac{\partial H}{\partial p_i} = \frac{\partial K(p)}{\partial p_i}, \quad \frac{\partial p_i}{\partial t} = \frac{\partial H}{\partial q_i} = -\frac{\partial U(q)}{\partial q_i} \tag{14}$$

Q is the position, P is the momentum, and each state in HMC is expressed in two dimensions. The reasons why HMC can solve the random walk and low rejection rate of MH are as follows: (a) continuous Hamiltonian dynamic has the property of conversation of Hamiltonian, that is $-\mathrm{H}(\mathrm{Q}*, \mathrm{P}*) + \mathrm{H}(\mathrm{Q}, \mathrm{P}) = 0$, and the rejection rate is 0. In general, the rejection rate of HMC is much lower than that of other algorithms. (b) The existence of momentum P can control the velocity of motion in one state. P is updated in every iteration. The uncertainty of P makes it more likely to transfer from one state to a far state, which can suppress random walk behavior. To reduce the computational complexity of the gradient, the stochastic gradient is generated.

The SGHMC algorithm is based on the Hamiltonian dynamics method, which combines dynamic equations with random perturbation terms with the random gradient descent algorithm to perform Monte Carlo sampling in high-dimensional parameter space and gradually approximate the target distribution $p(\boldsymbol{\theta})$. The following is a process description of the Stochastic Gradient Hamiltonian Monte Carlo (SGHMC) method.

Input: Target distribution $p(\boldsymbol{\theta})$, data $\mathbf{X}$, hyperparameter α, learning rate ϵ, mass matrix $\mathbf{M}$, and stochastic gradient estimate $\mathbf{g}(\boldsymbol{\theta})$.

Output: Sampled parameters $\boldsymbol{\theta}_{1:S}$.

1) Initialize $\boldsymbol{\theta} \leftarrow \boldsymbol{\theta}_0$ and $\mathbf{v} \sim \mathcal{N}(0, \mathbf{M})$, where $\mathbf{M}$ is a predefined mass matrix.
2) Repeat the following process S times:
   - Sample a mini-batch $\mathbf{X}_{\text{batch}}$ randomly from the data.
   - Compute the stochastic gradient estimate $\mathbf{g}(\boldsymbol{\theta})$.
   - Sample a Gaussian noise $\eta \sim \mathcal{N}(0, 2\alpha\epsilon\mathbf{M})$.
   - Update the velocity $\mathbf{v} \leftarrow (1 - \alpha)\mathbf{v} - \epsilon\mathbf{g}(\boldsymbol{\theta}) - \eta$.
   - Update the position $\boldsymbol{\theta} \leftarrow \boldsymbol{\theta} + \mathbf{v}$.
3) Output $\boldsymbol{\theta}_{1:S}$.

See the paper [15] for the complete HMC algorithm and SGHMC algorithm flow.

Figure 7 contrasts the sampling effects of two sampling techniques, Metropolis Hastings and SGHMC, on a two-dimensional Gaussian distribution. The effectiveness of Metropolis Hastings and SGHMC sampling methods can be visually compared. The samples obtained from Metropolis Hastings are more diffuse than those obtained from SGHMC. Compared to SGHMC, the Metropolis Hastings (MH) sample has the following disadvantages:

MH sampling necessitates the calculation of acceptance probability, and in cases of low acceptance rate, multiple

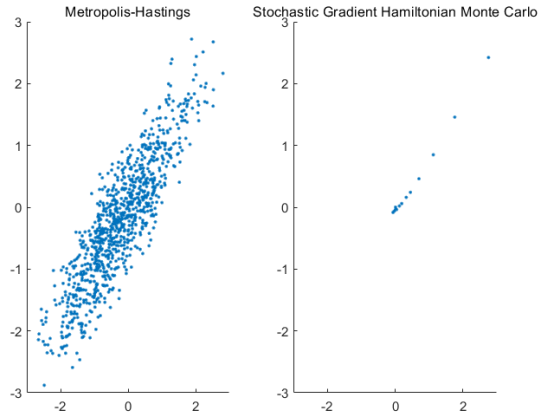

FIGURE 7. This image samples a two-dimensional Gaussian distribution using two sampling methods, Metropolis Hastings and SGHMC.

resamples are required, resulting in relatively low sampling efficiency. SGHMC can utilize random gradient information for sampling, thereby averting the disadvantage of calculating the full gradient each time and enhancing sampling efficiency.

Adjustments must be made to the potential distribution: The effectiveness and outcomes of MH sampling are highly dependent on the selected potential distribution. If the proposal distribution is too scattered or too concentrated, the acceptance rate will be low, which will o randomly sample an initial valimpact sampling efficiency and results. SGHMC can modify the step size and mass matrix adaptively to accommodate various target distributions and data sets.

Since the acceptance rate of MH sampling is only related to the current position and prospective distribution, and not the previous sampling path, difficult to control convergence issues are likely to arise. If the proposal distribution is not properly selected, the sampling path may oscillate repeatedly in low-density regions, resulting in delayed convergence. The SGHMC algorithm has improved convergence because it includes the momentum term in sampling, thereby avoiding the issue of repeated oscillations in low density regions and making convergence simpler to achieve. In addition, SGHMC can enhance sampling quality through hyperparameter adjustment.

SGHMC is more suitable for sampling large-scale datasets and complex target distributions due to its superior sampling efficiency, convergence, and adaptability in comparison to MH.

IV. CALCULATION OF POSTERIOR PARAMETER DISTRIBUTIONS

In Equation (4), we want to find the value of the parameter a in the linear equation $y = \mathbf{x}^T\theta$. We have five possible values for θ. To solve this problem, we can use the posterior distribution, which is proportional to the likelihood function multiplied by the prior distribution.

$$p\left(\theta, \tau^2 \mid \mathbf{y}\right) = \frac{p\left(\mathbf{y} \mid \mathbf{X}, \theta, \tau^2\right) p(\theta) p\left(\tau^2\right)}{p(\mathbf{y})} \propto p\left(\mathbf{y} \mid \mathbf{X}, \theta, \tau^2\right) p(\theta) p\left(\tau^2\right) \tag{15}$$

In Equation (15), $p(\theta, \tau^2|\mathbf{y})$ is the posterior distribution of the parameters θ and τ^2 given the observed data $\mathbf{y}$, where θ represents the five position parameters in the linear model $y = \mathbf{x}^T\theta$, and τ^2 represents the variance of the residuals. The objective is to estimate θ and τ^2 using $\mathbf{y}$ and prior knowledge regarding the distributions of θ and τ^2.

This formula represents the posterior distribution of parameters θ and τ^2 given the observed data $\mathbf{y}$. It is obtained by applying Bayes' theorem to the likelihood function $p(\mathbf{y} \mid \mathbf{X}, \theta, \tau^2)$ and prior distributions $p(\theta)$ and $p(\tau^2)$ of the parameters. The denominator $p(\mathbf{y})$ is a normalization constant that ensures that the posterior distribution is a valid probability distribution. $\propto$ indicates that the right-hand side is proportional to the left-hand side up to the normalization constant. The selection of prior parameter distributions is a method for choosing prior distributions for *theta* and τ^2 based on prior knowledge or assumptions regarding the parameters.

$$\begin{aligned} p\left(\theta, \tau^2 \mid \mathbf{y}\right) &\propto p\left(\mathbf{y} \mid \mathbf{X}, \theta, \tau^2\right) p(\theta) p\left(\tau^2\right) \\ &\propto \prod_{i=1}^{N} \mathcal{N}\left(y_i \mid \mathbf{x}_i^T\theta, \tau^{-2}\right) \prod_{j=1}^{5} \mathcal{N}\left(\theta_j \mid 0, 1\right) \\ &\quad \cdot \text{Inv-Gamma}\left(\tau^2 \mid 2, 2\right) \end{aligned} \tag{16}$$

This Equation (16) is the posterior distribution of the parameters θ and τ^2 given the observed data $\mathbf{y}$, which is proportional to the likelihood of the data times the prior distributions of θ and τ^2.

The likelihood function describes the probability of observing the data $\mathbf{y}$ given the parameters θ and τ^2. This means that the values in the data are assumed to be generated by adding random noise to a linear combination of the input variables $\mathbf{x}_i$ weighted by the parameters θ, and that the magnitude of the noise is controlled by the parameter τ^2.

The prior distributions for θ are assumed to be normal distributions with mean zero and variance one, and the prior distribution for τ^2 is an inverse gamma distribution with parameters (2, 2).

By multiplying the likelihood and prior distributions together and simplifying, we get a proportional expression that is proportional to the posterior distribution. Finally, the resulting expression is a product of a power of τ, an exponential function of τ^2, and a Gaussian distribution of θ in (20), as shown at the bottom of page 20.

By experimenting and adjusting the initial parameter values, one can achieve satisfactory results. Typically, it is possible to select an initial value that is close to the true value or to randomly sample an initial value from a prior distribution. Please refer to Appendix A.B for the initial values of the procedure for determining the shape and scale parameters and

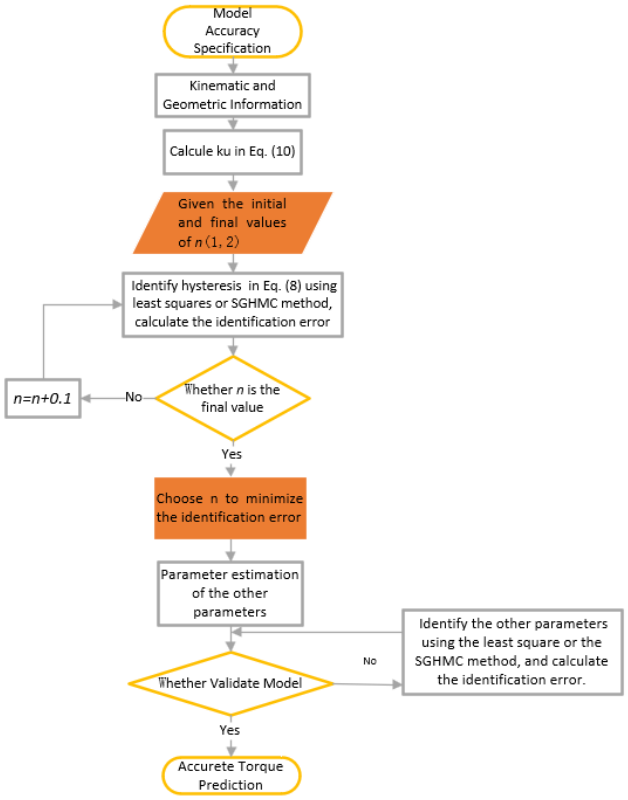

FIGURE 8. A standard experimental robot identification procedure is schematically represented in figure.

the inverse gamma prior parameters. The Appendix A.A is the specific derivation of the (16).

V. RESULTS AND DISCUSSION

A standard experimental robot identification procedure is schematically represented in the Figure 8. The procedure takes inputs such as the kinematic and geometric information of the robot manipulator, as well as model-accuracy specifications. These inputs, known before the identification process, guide the choices made during the procedure. The model validation step assesses the accuracy of the identified model based on criteria. If the identified model fails the validation tests, the procedure may be repeated.

In Figure 8, the procedure takes inputs such as the kinematic and geometric information of the robot manipulator, as well as model-accuracy specifications. These inputs, known before the identification process, guide the choices made during the procedure. The model validation step assesses the accuracy of the identified model based on criteria. If the identified model fails the validation tests, the procedure may be repeated. In Figure 8, the parameter n is considered to be sensitive according to reference [46]. This implies that, when other parameters are held constant, a small change in n has a big effect on the model. Specifically, the parameter n influences the smoothness of the Bouc-Wen curve, but it does not impact other characteristics. Therefore, the value of n can be constrained to a natural number within a specific range, depending on the particular circumstances.

Based on the analysis above, it is evident that the restoring force is significantly affected by the parameter n. Consequently, n can be limited to a specific natural number value. Additionally, we can calculate the value of k_u using the information provided in reference [47]. According to the paper, when the loading displacement exceeds five times the yield displacement, the restoring force R demonstrates almost linear behavior concerning the loading displacement. At this point, the parameter k_u can be expressed as $\Delta R/\Delta x$, where ΔR represents the change in restoring force and Δx represents the change in loading displacement.

Below, we summarize the details of the experimental setup and parameter identification, along with information regarding the duration of the experiment and computational complexity.

1) Implementation:
   - Programming Language and Development Environment: MATLAB R2021b
   - Tools: MATLAB's Signal Processing Toolbox, Optimization Toolbox
2) Validation Procedure:
   - Experimental Setup:
     a) Hardware: CMOR (CFETR Multipurpose Overload Robot) robot system and associated hardware.
     b) Measurement Instruments: Measurement instruments and sensors used in the CMOR single joint (fourth joint) experimental platform.
   - Parameter Identification Steps:
     a) Use the composite link method to determine the dynamic characteristics of each identifiable part.
     b) Optimize the Fourier series parameters [38], [39] as excitation trajectories by minimizing the logarithm of the condition number of the observation matrix in the motion equations.
   - Algorithm: Parameter Identification based on SGHMC Algorithm
     a) Input: Parameter data for identification
     b) Define the prior distribution of the parameters, including prior mean and variance.
     c) Initialize parameter values using the prior distribution's mean as the initial value.
     d) Define the step size and iteration count.
     e) Define the hyperparameters of the SGHMC algorithm, including the noise variance of stochastic gradient estimation and the coefficient of friction.
     f) Generate candidate parameter values iteratively.
     g) Compute the posterior distribution of the parameters, including mean and variance, using the obtained samples.

h) Output the parameter identification results, using the mean of the posterior distribution as the final parameter estimate.

- Data Acquisition:
  a) Experimental Design 1: Measurement of joint output torque variation with speed and load.
  b) Experimental Design 2: Measurement of joint current and torque variation over time.
  c) Experimental Design 3: Excitation trajectory using Fourier functions.
- Validation Time:
  a) Duration of the experiment: 10 days
  b) Individual step time: Time taken for the robot arm to rotate 180 degrees, determined by the rotation speed.
- Computational Complexity:
  – Algorithm: Parameter Identification based on SGHMC Algorithm
  – Time Complexity:
    a) The time complexity of an algorithm depends on its implementation and computation stages. The general time complexity for parameter identification based on the SGHMC algorithm can be broken down into the following steps:
      i) Parameter Initialization: $O(1)$ time complexity.
      ii) Generation of Candidate Parameter Values: Time complexity is primarily dependent on the sampling algorithm employed, such as the HMC algorithm, which has a typical time complexity of $O(M)$, where M is the number of sampling steps.
      iii) Gradient Calculation of the Objective Function: In general, the time complexity is $O(N)$, where N is the number of data samples and depends on the form and calculation method of the objective function.
      iv) Parameter Update: In general, parameter updating has a time complexity of $O(1)$ or $O(D)$, where D is the dimension of the parameters, depending on the method and computational complexity.
      v) Multiple parameter updates are implemented based on the predetermined number of iterations or other halting criteria. Typically, the iteration procedure has a time complexity of $O(K)$, where K is the number of iterations.
    b) In conclusion, the time complexity of parameter identification based on the SGHMC algorithm is determined by the generation of candidate parameter values and the computation of the objective function's gradient, which has time complexities of $O(M)$ and $O(N)$, respectively.

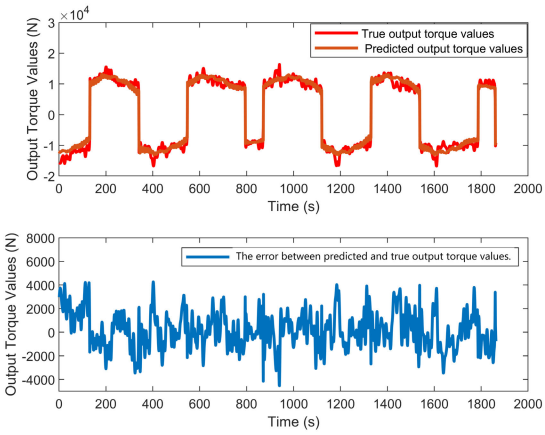

FIGURE 9. True output torque values and SGHMC predicted output torque values in (4).

TABLE 3. The results of the Least Square method and SGHMC method in (4).

Parameter	Description	Unit	Least Square	SGHMC	95% Credible Interval
1	I_{xx}	kg · m^2	6685.166	6681.266	[6599.640, 6753.321]
2	mr_x	kg · m	20.779	20.780	[19.302, 22.305]
3	mr_y	kg · m	-34.543	-34.523	[-38.549, -30.420]
4	f_v	N · s/m	8683.272	8682.911	[8663.980, 8702.206]
5	f_c	N	2352.660	2352.936	[2332.964, 2372.455]

We utilize RMSE as the metric for evaluating the error, which serves as a measure of the overall deviation between the predicted and actual values.

$$\mathrm{RMSE} = \sqrt{\frac{1}{n}\sum_{i=1}^{n}\left(y_i - \hat{y}_i\right)^2} \tag{17}$$

where n is the number of observations, y_i is the true value, $\hat{y}_i$ is the predicted value.

A. POSTERIOR PARAMETER DISTRIBUTIONS AND ANALYSIS OF MODEL PREDICTION UNCERTAINTY

1) POSTERIOR PARAMETER DISTRIBUTIONS OF (4)

In Table 3 parameters 1 to 5 represent the following variables: I_{xx} (Moment of inertia around the X-axis), mr_x (Product of mass and distance along the X-axis), mr_y (Product of mass and distance along the Y-axis), f_v (Viscous friction coefficient), and f_c (Coulomb friction coefficient).

The RMSE between the predicted output torque values using the SGHMC method estimated values and true output torque values is 2227.144.

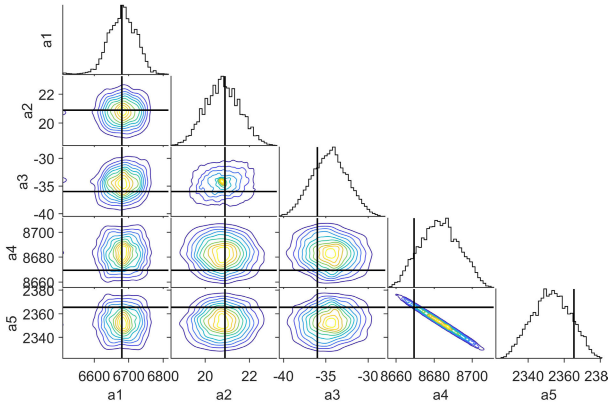

FIGURE 10. This image plots the corner plot of the posterior distributions in (4).

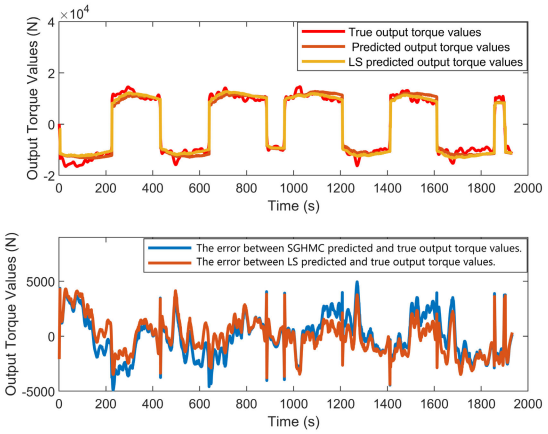

FIGURE 11. True output torque values, SGHMC method and Least square method predicted output torque values in (11).

The RMSE between the predicted output torque values using the LS method estimated values and true output torque values is 2227.144.

Figure 9 displays the comparison between the true output torque values and the predicted output torque values obtained using the SGHMC method for Equation (4). The graph illustrates that the SGHMC predictions closely align with the true values, indicating the method's effectiveness in accurately estimating the output torque. In Figure 10, the corner plot showcases the posterior distributions of the parameters in Equation (4) obtained through the SGHMC method. The plot provides valuable insights into the uncertainties and correlations between the parameters, aiding in a comprehensive understanding of the system's dynamics.

Table 3 presents the results of the Least Square (LS) method and the SGHMC method for Equation (4). The table highlights the estimated values for the parameters, along with their respective 95% credible intervals. It can be observed that the SGHMC method yields parameter estimates that are close to those obtained from the LS method.

2) POSTERIOR PARAMETER DISTRIBUTIONS OF SGHMC IN (11)

The parameters 1 to 5 in Table 4 are: k_u (Proportional gain for input $u(t)$), k_h (Proportional gain for input $x(t)$), f_v (Viscous friction coefficient), $D + f_c$ (Sum of viscous friction coefficient and inertia), and C (Constant term) in (11).

The RMSE between the predicted output torque values using the SGHMC method estimated values and true output torque values is 1705.926.

The RMSE between the predicted output torque values using the LS method estimated values and true output torque values is 1845.883.

Figures 11 and 12, along with Table 4, display the outcomes of LS and SGHMC methods applied to identify parameters in Equation (10). Figure 11 illustrates the comparison between the true output torque values and the predicted output torque values obtained using both the SGHMC method and the Least Square (LS) method for Equation (11). The graph

TABLE 4. The results of the Least square method and SGHMC method in (11).

Parameter	Description	Unit	Least square	SGHMC	95% Credible Interval
1	k_u	-	-761.529	-689.076	[-1501.594, 16.680]
2	k_h	-	16909.986	16987.952	[16027.840, 17666.666]
3	f_v	Nm/(m/s)	9069.448	9305.415	[8137.896, 10057.360]
4	$D + f_c$	Nm/(m/s)	492.014	375.168	[-711.280, 1582.123]
5	C	Nm	-492.237	-412.486	[-1520.071, 631.033]

demonstrates that the SGHMC method achieves a closer fit to the true values compared to the LS method, indicating its superior performance in estimating the output torque accurately.

In Figure 12, the plot showcases the posterior distributions of the parameters in Equation (11) obtained through the SGHMC method. This visualization provides valuable insights into the uncertainties associated with the parameter estimates and facilitates a comprehensive understanding of their distributions.

Table 4 presents the results of the LS method and the SGHMC method for Equation (11). The table displays the estimated values for the parameters, along with their respective 95% credible intervals. It can be observed from the table the effectiveness of the SGHMC method. The provided RMSE values of 1705.926 and 1845.883 indicate the respective accuracies of the SGHMC and LS methods in predicting the output torque.

3) EFFICIENCY COMPARISON OF MCMC AND SGHMC METHOD: MEAN AUTOCORRELATION AND RHAT

The provided Figure 13 shows the comparison between the true output torque and the predicted output torque obtained using the MCMC method in (11). The table in Table 5 presents the results of the MCMC method, including the

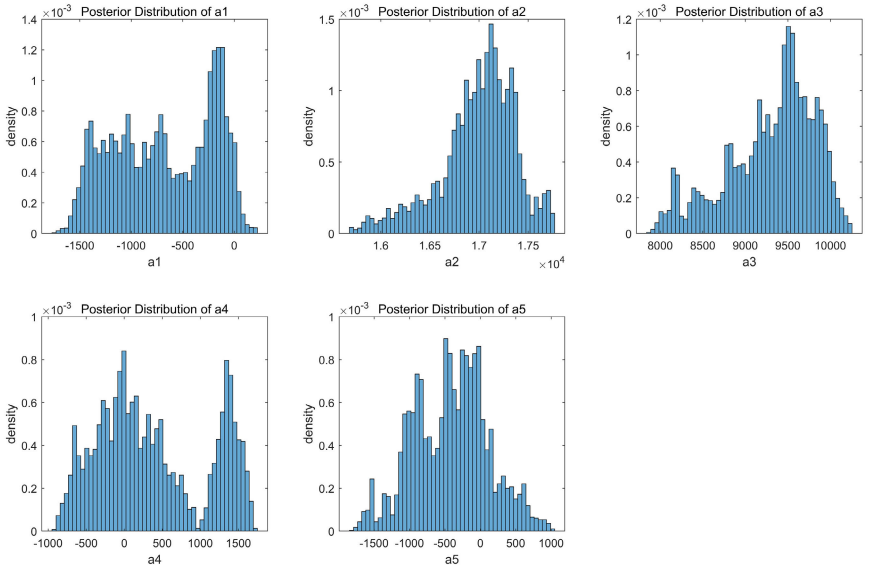

FIGURE 12. This image plots the posterior distributions in (11).

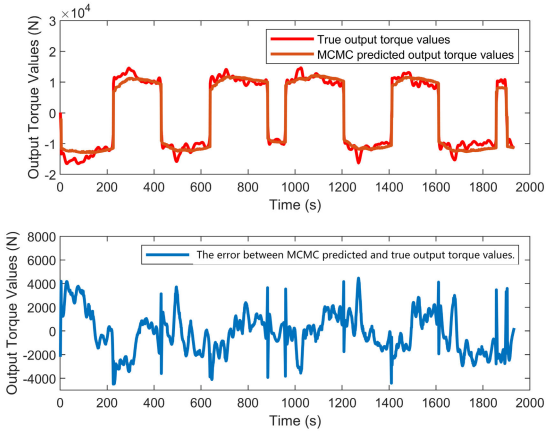

FIGURE 13. This image plots the true output torque and the MCMC method predicted output torque in (11).

TABLE 5. The results of MCMC Method in (11).

Parameter	Description	Unit	MCMC	95% Credible Interval
1	k_u	-	-714.487	[-766.713, -666.645]
2	k_h	-	16921.728	[16876.993, 16953.551]
3	f_v	Nm/(m/s)	9051.270	[9023.947, 9079.557]
4	$D+f_c$	Nm/(m/s)	475.074	[436.007, 511.528]
5	C	Nm	-587.327	[-642.374, -503.742]

TABLE 6. Mean Autocorrelation values for MCMC and SGHMC method.

No.	1	2	3	4	5
MCMC	0.7×10^{-3}	-0.8×10^{-3}	3.4×10^{-3}	-0.2×10^{-3}	1.9×10^{-3}
SGHMC	-0.599×10^{-3}	0.679×10^{-4}	-0.93×10^{-5}	0.293×10^{-3}	-0.747×10^{-4}

estimated parameter values and their corresponding 95% credible intervals. The root mean squared error (RMSE) between the predicted output torque values (based on the estimated parameter values) and the true output torque values is 1741.990.

The figure visually demonstrates the agreement between the predicted and true output torque, indicating that the MCMC method captures the underlying patterns reasonably well. The relatively small RMSE value suggests that the MCMC method provides accurate predictions with a reasonable level of precision.

Overall, based on the visual comparison, parameter estimates, interval estimates, and RMSE, the MCMC method shows promising performance in predicting the output torque.

We calculate the autocorrelation of the samples obtained from both algorithms and compare them. Lower autocorrelation indicates a higher efficiency, as it implies that subsequent samples are less dependent on each other. The autocorrelation function is in the third chapter of this article [48].

Based on the average autocorrelation values and in the provided figures 14 and 15, it can be observed that the SGHMC algorithm has relatively smaller values compared to the MCMC algorithm. The values range from -0.5994e-03 to 0.2927e-03 for SGHMC, while MCMC has values ranging from -0.0008 to 0.0034.

This suggests that the SGHMC algorithm exhibits faster convergence and better mixing properties compared to the MCMC algorithm. The smaller autocorrelation values indicate that the samples generated by SGHMC are less correlated and reach stationarity more quickly. This can lead to

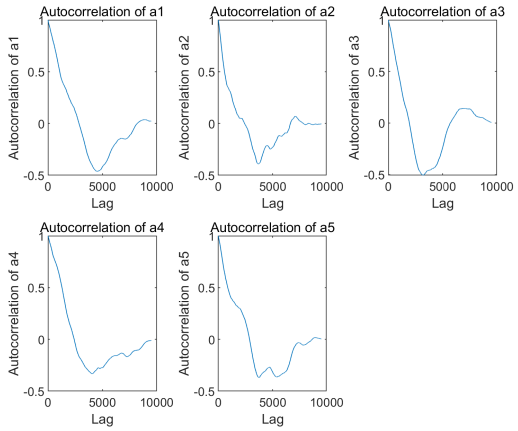

FIGURE 14. The autocorrelation values of the samples obtained from SGHMC algorithm in (11).

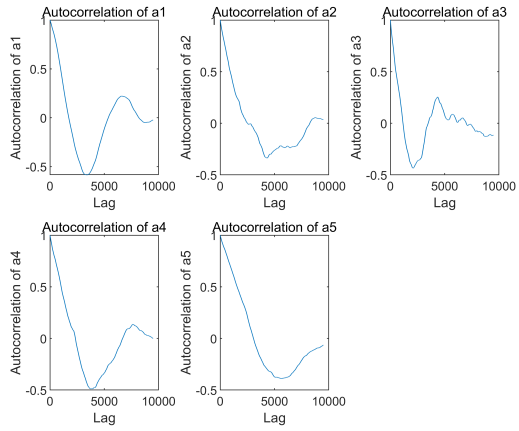

FIGURE 15. The autocorrelation values of the samples obtained from MCMC algorithm in (11).

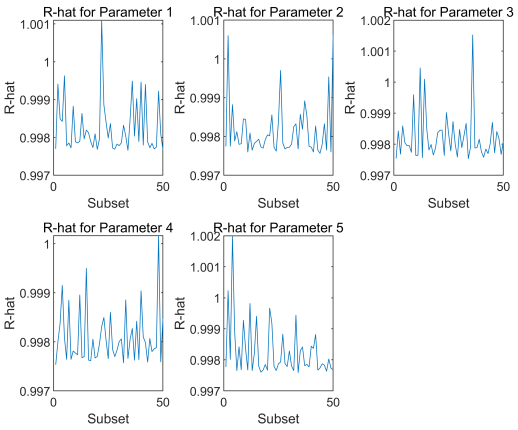

FIGURE 16. The RHat values of SGHMC algorithm of the samples obtained from the (11).

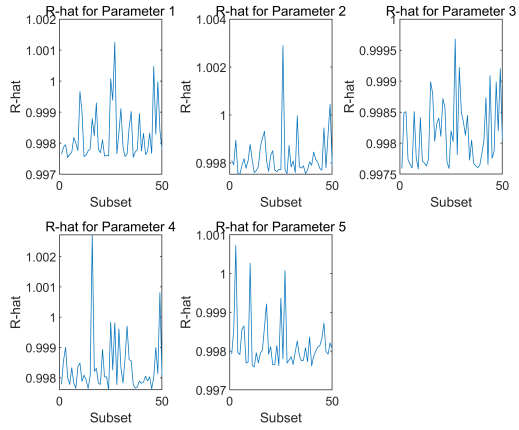

FIGURE 17. The RHat values of MCMC algorithm of the samples obtained from the (11).

more efficient exploration of the parameter space and faster convergence to the target distribution. In summary, based on the average autocorrelation values, the SGHMC algorithm demonstrates faster convergence compared to the MCMC algorithm. The smaller autocorrelation values indicate faster exploration of the parameter space in SGHMC.

The Gelman-Rubin convergence statistic (RHat) [49] is commonly used to assess the convergence of Monte Carlo chains. It provides a measure of how well multiple chains agree with each other and whether they have reached convergence to the desired distribution. In general, RHat values below 1.1 indicate that the chains have converged. Therefore, values of RHat less than 1.1 are typically considered indicative of satisfactory convergence to the desired distribution.

Compare the number of iterations required for both algorithms to converge to a reasonable estimate of the target distribution. In the provided figures 16 and 17 and Table 7, the number of iterations for both algorithms is set to 10000. We calculate the Rhat value every 200 points. By observing the convergence behavior, we can assess which algorithm converges faster. According to the calculation results, the RHat values of both MCMC and SGHMC algorithms are close to 1, indicating that they have good convergence in parameter estimation.

However, from the results, the RHat value of the SGHMC algorithm is relatively slightly lower, indicating that it may be slightly better than the MCMC algorithm in terms of convergence speed. This may be because the SGHMC algorithm introduces randomness when updating parameters and utilizes stochastic gradient estimation to speed up the convergence process. In contrast, the MCMC algorithm uses Metropolis-Hastings sampling, and its update process is relatively conservative.

Overall, the SGHMC algorithm may achieve better convergence in a shorter number of iterations, while the MCMC algorithm may require more iterations to achieve similar results.

4) POSTERIOR PARAMETER DISTRIBUTIONS OF SGHMC IN (9)

The parameters 1 to 3 in Table 8 represent the following variables: α (the shape constant of the hysteresis curve),

TABLE 7. RHat average values for MCMC and SGHMC.

Parameter	1	2	3	4	5
MCMC	0.9982	0.9982	0.9984	0.9983	0.9984
SGHMC	0.9983	0.9981	0.9982	0.9981	0.9983

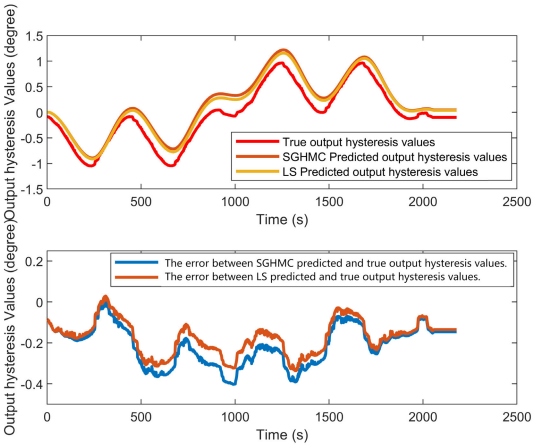

FIGURE 18. True hysteresis values, the SGHMC method, and Least square method predicted hysteresis values in (9).

TABLE 8. The results of the Least square method and SGHMC method in (9).

Parameter	Description	Least square	SGHMC	95% Credible Interval
1	α	0.003	0.040	[-0.028, 0.121]
2	β	0.002	0.012	[-0.047, 0.072]
3	γ	-0.042	-0.011	[-0.160, 0.149]

β (the shape constant of the hysteresis curve), and γ (the shape constant of the hysteresis curve) in equation (9). They are coefficient factors that affect the behavior of the equation, so they do not have specific units of measurement.

Determine n=1 first, and then proceed with the calculation, as a slight change in the value of n will result in a significant change in the results of hysteresis. The sensitivity analysis will be conducted in the next section.

The RMSE between the predicted hysteresis values using the SGHMC method estimated values and true hysteresis values is 0.234. The RMSE between the predicted hysteresis values using the LS method estimated values and true hysteresis values is 0.545.

Lastly, Figures 18, 19, and 20, along with Table 8, exhibit the results of LS and SGHMC methods for parameter identification in Equation (9).

Figure 18 showcases the comparison between the true hysteresis values and the predicted hysteresis values obtained using the SGHMC method and the Least Square (LS) method for Equation (9). It can be observed that the SGHMC method provides a closer match to the true values compared to the LS method, indicating its superior performance in accurately estimating the hysteresis behavior of the system.

In Figure 19, the corner plot of the posterior distributions for Equation (9) is displayed. This plot provides a comprehensive visualization of the uncertainties associated with the estimated parameters. By examining the intersections of the histograms, valuable insights can be gained regarding the correlations and probability distributions of the parameters. Figure 20 presents the posterior distributions for Equation (9). This plot provides a detailed representation of the probability density functions for each parameter.

Table 8 summarizes the results obtained from the LS method and the SGHMC method for Equation (9). The table displays the estimated values for the parameters, along with their respective 95% credible intervals. It can be observed that the SGHMC method yields parameter estimates that differ from those obtained by the LS method. The RMSE values represent the prediction accuracy of the SGHMC and LS methods when estimating hysteresis values, respectively. The SGHMC method exceeds the LS method in capturing the hysteresis behavior of the system, which is shown by a lower RMSE value.

5) DISCUSSIONS

RMSE (Root Mean Square Error) is a commonly used evaluation indicator in a variety of disciplines, including statistics and data analysis. It provides a quantitative evaluation of the accuracy of a predictive model or estimation technique by measuring the average difference between predicted and actual values.

The significance of RMSE resides in its capacity to provide an all-encompassing measure of prediction error. This characteristic makes RMSE particularly valuable in situations where balanced performance between positive and negative errors is desired.

RMSE is expressed in the same units as the variable being predicted, making it simple to interpret. This makes it easy for researchers, practitioners, and decision-makers to comprehend the magnitude of prediction errors in terms of their actual impact.

In this study, the RMSE values reveal the accuracy of the SGHMC and LS methodologies in estimating output torque and hysteresis values. A smaller RMSE suggests a better fit between the predicted and actual values, indicating greater precision and dependability of the respective methods. Comparing the RMSE values allows for the evaluation and comparison of the effectiveness of the two methods in capturing the dynamics and hysteresis effects of the under investigation robotic system.

This article primarily focuses on the application of the SGHMC method, therefore only one formula is used for comparing the efficiency of MCMC and SGHMC. Other formulas are not repeatedly compared between the two methods.

To evaluate the performance of the SGHMC method, a single formula is chosen for comparison against the MCMC method. The results obtained from this formula are presented in Table 4. The SGHMC method demonstrates competitive efficiency in estimating the parameters, as indicated by the

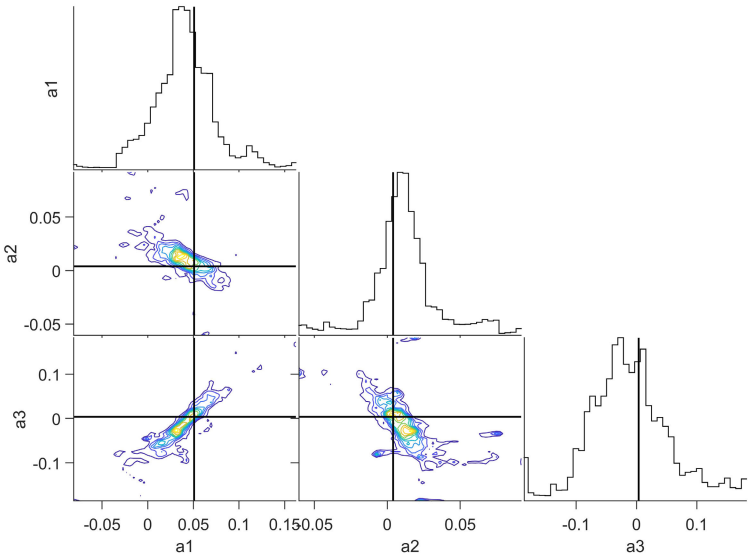

FIGURE 19. This image plots the corner plot of the posterior distributions in (9).

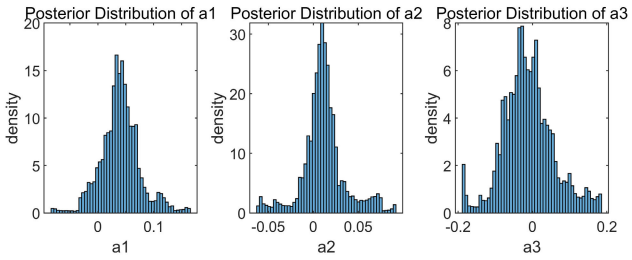

FIGURE 20. This image plots the posterior distributions in (9).

TABLE 9. Root Mean Square Error (RMSE) Comparison. The table compares the RMSE values for the output torque values predicted by the SGHMC method and the LS method for two distinct equations. Equation (4) represents the model of the robot's dynamics based on LaGrange, while Equation (11) represents the model devised to describe the hysteresis effect based on the Bouc-Wen (CBW) model.

Equation	SGHMC Method	LS Method
(4)	2227.144	2227.144
(11)	1705.926	1845.883

comparable values of the Gelman-Rubin convergence statistic (RHat) and the mean autocorrelation.

By focusing on a specific Equation (11), the article emphasizes the effectiveness of the SGHMC method in tackling the targeted problem. The comparative analysis of RHat and mean autocorrelation highlights the convergence speed and independence of samples generated by the SGHMC method. This approach allows for a comprehensive evaluation of the SGHMC method's performance without redundant comparisons across multiple formulas.

Overall, the SGHMC method shows better results and proves to be a viable alternative to the MCMC method for the specific formula considered in this study.

The study of section V-A found that the SGHMC algorithm outperformed the Least Square method for computing the robot arm's output torque in terms of precision. This result indicates that SGHMC can be an effective instrument for solving complex optimization problems, especially those involving large datasets or high-dimensional parameter spaces.

By comparing the root mean square error (RMSE) of the predicted output torque of the SGHMC method and the LS method on two different equations, we observed that the RMSE of the two methods in equation (4) is the same as 2227.144, while in equation (11) The RMSE of the SGHMC method is 1705.926, and the RMSE of the LS method is 1845.883. The results show that the SGHMC method has better predictive performance on Equation (11). The RMSE reduction of the GHMC method on equation (11) is about 8.16%.

In this study, two different models, Equation (4) based on the Lagrange formulation and Equation (11). based on the Bouc-Wen (CBW) model, were employed to capture the dynamics and hysteresis effect of the robotic arm. In Table 9, a comparison of the calculation results using these equations was presented, with Equation (9) focusing on modeling the hysteresis phenomenon itself.

Figures 9 and 10, along with Table 3, displayed the results of parameter identification using the LS and SGHMC methods for Equation (4). Figure 9 showed that the SGHMC method accurately estimated the output torque, closely aligning with the true values. The corner plot in Figure 10 provided insights into parameter uncertainties and correlations, aiding in understanding the system's dynamics. Table 3 highlighted that the SGHMC method yielded parameter estimates close to those obtained from the LS method.

Similarly, Figures 11 and 12, along with Table 4, presented the outcomes of LS and SGHMC methods applied to identify parameters in Equation (11). Figure 11 demonstrated that the SGHMC method outperformed the LS method in accurately estimating the output torque. The posterior distributions in Figure 12 provided a comprehensive understanding of parameter uncertainties. Table 4 showcased the effectiveness of the SGHMC method, with lower RMSE values indicating its superior performance in predicting the output torque compared to the LS method.

Lastly, Figures 18, 19, and 20, along with Table 8, exhibited the results of LS and SGHMC methods for parameter identification in Equation (9). Figure 18 showed that the SGHMC method achieved a closer match to the true hysteresis values compared to the LS method. The corner plot in Figure 19 provided insights into parameter uncertainties and correlations, while Figure 20 displayed the posterior distributions, representing the probability density functions for each parameter. Table 8 summarized the results, indicating that the SGHMC method outperformed the LS method in estimating the hysteresis values, as reflected by the lower RMSE value.

Overall, the SGHMC method demonstrated superior performance in accurately estimating the output torque and capturing the hysteresis behavior of the robotic arm, as evidenced by the close alignment with true values and lower RMSE values compared to the LS method. These findings emphasize the effectiveness of the SGHMC algorithm in parameter estimation for robotic arm systems.

Regarding parameter estimation and model selection, the SGHMC algorithm exhibits outstanding computational efficiency and accuracy. This study demonstrates that the SGHMC algorithm is a powerful modeling and parameter estimation tool for dynamic systems with complex structures. In addition, we observe that the Least-squares algorithm can provide a high level of precision and efficiency under certain conditions, especially for simple linear models. Therefore, selecting an appropriate algorithm depends on the nature of the problem and the data, and requires trade-offs and decisions based on the situation.

B. ANALYSIS OF FIRST-ORDER SENSITIVITY INDEX AND GLOBAL SENSITIVITY

1) FIRST-ORDER SENSITIVITY INDEX AND GLOBAL SENSITIVITY OF (4)

The "First-order sensitivity index", or "main effect index" is stated in [50]. The "Total-effect index" or "Total-order index" is stated in [51]. The First order sensitivity index can be used to analyze the impact of parameters in SGHMC identification on the output, thereby optimizing the parameter configuration of SGHMC by determining which parameters have a significant impact on the output. By calculating the first-order sensitivity index of each parameter, we can evaluate each parameter's contribution to the output variance, thereby gaining a deeper understanding of the SGHMC model and its parameters. Utilizing the first-order sensitivity index in the tuning of SGHMC can direct parameter adjustments toward improved model performance.

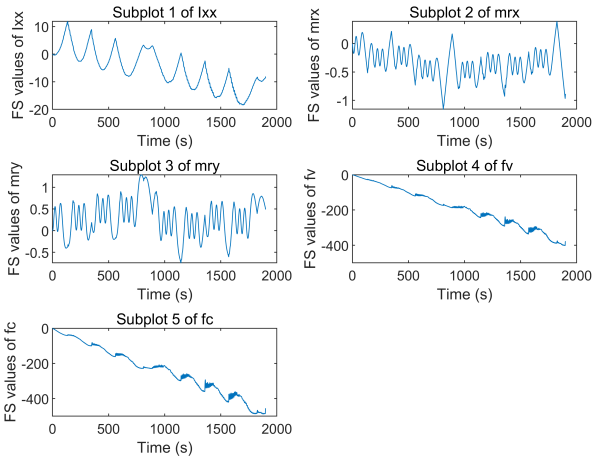

FIGURE 21. First-order sensitivity index values in (4). Subplot1: First-order sensitivity index of I_{xx} (Moment of inertia around the X-axis) Subplot2: First-order sensitivity index of mr_x (Product of mass and distance along the X-axis) Subplot3: First-order sensitivity index of mr_y (Product of mass and distance along the Y-axis) Subplot4: First-order sensitivity index of f_v (Viscous friction coefficient) Subplot5: First-order sensitivity index of f_c (Coulomb friction coefficient).

The first-order sensitivity index for parameter X_i can be calculated using the following formula:

$$FS_i = \frac{\mathrm{Var}\left(E\left(Y \mid X_i\right)\right)}{\mathrm{Var}(Y)} \tag{18}$$

where FS_i is the first-order sensitivity index, $\mathrm{Var}(E(Y|X_i))$ represents the variance of the conditional expectation of the output Y given the parameter X_i, and $\mathrm{Var}(Y)$ is the total variance of the output.

The Total effect index can assist in determining which parameters have the most significant effect on the model, especially when parameter interactions are present. Using the total effect index for sghmc can help determine which parameters have the greatest variance in the sample posterior distribution, which may necessitate additional data or more precise prior information to enhance estimation precision. Therefore, utilizing the total effect index is extremely useful for analyzing the parameters identified by sghmc, which can help us design experiments or construct models more effectively.

The total-effect index for parameter X_i can be calculated using the following formula:

$$T_i = \frac{\mathrm{Var}\left(E\left(Y \mid X_i\right)\right) + \sum_{j \neq i} \mathrm{Var}\left(E\left(Y \mid X_j, X_i\right)\right)}{\mathrm{Var}(Y)} \tag{19}$$

where T_i is the total-effect index, $\mathrm{Var}(E(Y|X_i))$ represents the variance of the conditional expectation of the output Y given the parameter X_i, $\mathrm{Var}(E(Y|X_j, X_i))$ represents the variance of the conditional expectation of the output Y given the parameters X_j and X_i together, and $\mathrm{Var}(Y)$ is the total variance of the output.

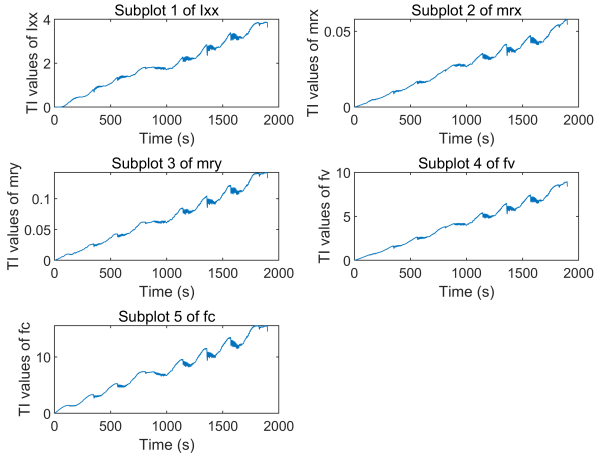

FIGURE 22. This image plots the Total-effect index in (4).Subplot1: Total-effect index of I_{xx} (Moment of inertia around the X-axis) Subplot2: Total-effect index of mr_x (Product of mass and distance along the X-axis) Subplot3: Total-effect index of mr_y (Product of mass and distance along the Y-axis) Subplot4: Total-effect index of f_v (Viscous friction coefficient) Subplot5: Total-effect index of f_c (Coulomb friction coefficient).

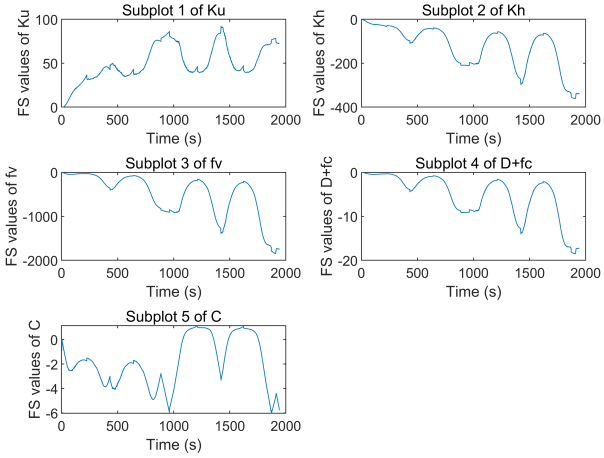

FIGURE 23. First-order sensitivity index values in (11). Subplot1: First-order sensitivity index of k_u (Proportional gain for input $u(t)$) Subplot2: First-order sensitivity index of k_h (Proportional gain for input $x(t)$) Subplot3: First-order sensitivity index of f_v (Viscous friction coefficient) Subplot4: First-order sensitivity index of $D + f_c$ (Sum of viscous friction coefficient and inertia) Subplot5: First-order sensitivity index of C (Constant term) in Equation (11).

In Figure 21 and Figure 22, we can see that the values of the Total effect index are sorted in descending order: $mr_x \approx f_v > f_c > I_{xx} > mr_y$. f_c and f_v are located in the second and third positions, so when considering the robotic arm as a rigid body, the frictional force has a significant impact on the output torque.

2) FIRST-ORDER SENSITIVITY INDEX AND GLOBAL SENSITIVITY OF SGHMC IN (11)

In Figure 23, we can see that the values of the First-order index are sorted in descending order: $f_v > K_h > K_u > D + f_c > C$. f_v is the fircton which is the maximum value. K_u is the proportional gain for input $u(t)$. K_h is the parameter

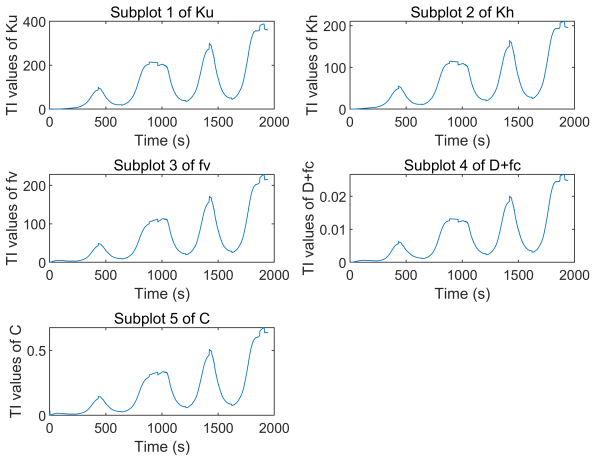

FIGURE 24. This image plots the Total-effect index in (11). Subplot1: Total-effect index of k_u (Proportional gain for input $u(t)$) Subplot2: Total-effect index of k_h (Proportional gain for input $x(t)$) Subplot3: Total-effect index of f_v (Viscous friction coefficient) Subplot4: Total-effect index of $D + f_c$ (Sum of viscous friction coefficient and inertia) Subplot5: Total-effect index of C (Constant term) in Equation (11). The subplots represent the total-effect indices of each parameter, indicating the overall influence of that particular parameter on the system's response or output.

of hysteresis deformation. In Figure 24 the values of Total effect index is sorted in descending order: $K_u > f_v \approx K_h > C > D + f_c$. It can be seen that hysteresis deformation has the greatest impact on the output torque.

The Total-Effect Index quantifies the global impact of a parameter on the model output. mr_x, f_v, f_c had the highest total-effect index for the first Equaiton (4), whereas K_u, f_v had the highest total-effect index for the second equation (11). This indicates that these parameters have a substantial effect on the model output and should be carefully considered when designing and controlling the robot arm.

VI. CONCLUSION

The results of this study demonstrate the efficacy of the SGHMC algorithm in parameter estimation for heavy-duty manipulators, making an important scientific contribution. This algorithm provides a robust and stable method for precisely estimating the system's parameters, thereby advancing the theoretical understanding of robotics. In addition, the practical implications of these findings are substantial, as the SGHMC algorithm demonstrates its efficacy in improving the reliability and performance of robotic arm systems in real-world applications. This research bridges the divide between theory and practice, paving the way for further investigation and development of advanced parameter estimation methods.

Based on calculations of the output torque of a heavy-duty robotic arm using the SGHMC and least squares algorithms, we discovered that the SGHMC algorithm with (11) produced the highest accuracy at a relatively lower computational cost. In addition, the analysis of the first-order and total-effect sensitivity indices revealed that mr_x, f_v, f_c, and $I_x x$ have the greatest influence on the output torque, followed by mr_y.

Moreover, the parameters K_u, f_v have significant effects on the respective output torque.

The effectiveness and efficacy of the SGHMC algorithm for analyzing the output torque of a heavy-duty robotic arm are demonstrated by our research. In addition, the sensitivity analysis offers valuable insights into the relative significance of various parameters and can steer the system's optimization.

This study's findings provide a foundation for future research into the use of SGHMC and the Total-Effect Index in robotics applications. In addition, only a limited number of model parameters were considered, and future research could investigate the sensitivity of the model output to a broader range of parameters.

The limitations of our research must be acknowledged. At first, the estimation of model parameters and sensitivity analysis relied on a restricted data set. A larger and more various data set would increase the scope and precision of our findings. Second, by concentrating on a particular set of model parameters, we may have overlooked other influential factors. Future research should investigate a broader range of parameters to achieve a deeper comprehension. Our analysis focused primarily on internal factors, ignoring external factors like temperature and disturbances. Including these variables in future research would result in a more accurate evaluation of the manipulator's performance in real-world situations.

The SGHMC method for parameter identification in heavy-duty manipulators confronts obstacles including the selection of suitable hyperparameters, the manipulation of high-dimensional parameter spaces, and the management of non-linear and complex dynamics. To ensure the efficacy and dependability of the SGHMC algorithm in accurately estimating the parameters of the robotic arm system, these obstacles must be carefully considered.

This investigation concludes with the development of a method for modeling and parameter estimation of the output torque of a heavy-duty robotic arm taking hysteresis deformation into account. This is crucial for solving and implementing practical problems.

Possible future directions include exploring the use of other random gradient methods, such as random gradient jumps. Finally, environmental factors, such as temperature, may affect the efficacy of the robot arm. Future research also holds the potential for explaining the performance of the SGHMC algorithm and other parameter estimation techniques in a wider range of application scenarios. Additional methods that effectively address model selection issues must be developed. In addition, it is essential to expand research on the SGHMC algorithm and other parameter estimation techniques to evaluate their efficacy in various application scenarios. To assure the heavy-duty manipulator's stability in a variety of conditions, it is essential to study the effect of environmental factors, such as temperature, on its performance. These research attempts will substantially improve the performance of robotic arms in the real world.

APPENDIX A
THE SPECIFIC DERIVATION OF THE POSTERIOR PARAMETER DISTRIBUTIONS

A. THE LIKELIHOOD FUNCTION AND PRIOR DISTRIBUTIONS

This Equation 17 represents the posterior distribution of parameters θ and τ^2 given the observed data $\mathbf{y}$. It is obtained by applying Bayes' theorem to the likelihood function $p(\mathbf{y} \mid \mathbf{X}, \theta, \tau^2)$ and prior distributions $p(\theta)$ and $p(\tau^2)$ of the parameters. The proportionality symbol $\propto$ indicates that the right-hand side is proportional to the left-hand side up to a normalization constant. The likelihood function assumes that the observed data $\mathbf{y}$ is normally distributed with a mean of $\mathbf{x}_i^T\theta$ and variance of τ^{-2}. The prior distributions for θ and τ^2 are assumed to be normal and inverse-gamma distributions, respectively. The posterior distribution is proportional to the likelihood function times the prior distributions. The selection of appropriate prior distributions is important for accurate Bayesian inference.

The specific calculation formula for the likelihood function $p(\mathbf{y} \mid \mathbf{X}, \theta, \tau^2)$ is as in (21), shown at the bottom of the next page.

B. THE METHOD OF DETERMINING THE PARAMETERS OF INVERSE GAMMA PRIOR

In Bayesian inference, the inverse-gamma prior distribution is commonly used as a conjugate prior for the precision or variance parameter in the normal distribution. This article [52] explores the benefits and applications of using an inverse gamma distribution as a prior distribution.

If y=ax finds parameter a, a is five parameters (same as Equation (4)), the mean value of x is known to be $n1$, the mean value of y is $n2$, and the variance is m^2, assuming that the prior distribution of a is an inverse Gamma distribution, the method of determining the shape parameter and scale parameter of inverse Gamma prior and the initial value of the parameter and the calculation process is given below.

$$p\left(a_i \mid \alpha_i, \beta_i\right) \propto \frac{\beta_i^{\alpha_i}}{\Gamma\left(\alpha_i\right)}\left(a_i\right)^{-\alpha_i-1} \exp\left(-\frac{\beta_i}{a_i}\right) \tag{22}$$

The Equation (22) represents the posterior distribution of the parameter a_i given the hyperparameters α_i and β_i in the inverse-gamma prior distribution $a_i \sim$ Inv-Gamma (α_i, β_i).

The mean and variance of the inverse gamma distribution are as follows:

$$\begin{aligned} E\left[a_i\right] &= \frac{\beta_i}{\alpha_i - 1}, \quad \alpha_i > 1 \\ \mathrm{Var}\left[a_i\right] &= \frac{\beta_i^2}{\left(\alpha_i - 1\right)^2\left(\alpha_i - 2\right)}, \quad \alpha \end{aligned} \tag{23}$$

The known variance m^2 is the variance of the prior distribution for each parameter a_i. In other words, when we set the inverse gamma distribution prior to each a_i, we can choose the appropriate shape parameter α_i and scale parameter β_i so that the variance of the prior distribution $Var[a_i]$ is equal to the known variance m^2.

TABLE 10. Design specifications of the fourth joint of CMOR.

Index	Output speed	Maximum output torque	Accuracy	Resolution	Angle range
Requirement	$\sim 0.03\text{rad/s}$	121.3kN	$\pm 0.02^\circ$	0.01°	$\pm 180^\circ$

TABLE 11. Test items and evaluation indicators of the test platform for the fourth joint of CMOR.

No.	Item	Parameter Index
1	Torque loading range	$0 \sim 180\text{kN} \cdot \text{m}$
2	Bending moment loading range	$0 \sim 250\text{kN} \cdot \text{m}$
3	Shear loading value	90kN
4	Bending moment load error	$\pm 2\text{kN} \cdot \text{m}$
5	Torque loading force error	$\pm 2\text{kN} \cdot \text{m}$
6	shear loading error	$\pm 2\text{kN}$

APPENDIX B
DESIGN SPECIFICATIONS OF THE FOURTH JOINT OF CMOR

Please refer to Table 10 and Table 11.

APPENDIX C
THE CONTROL SYSTEM DIAGRAM

The control system in Fig. 25 consists of a SIMATIC S7-1500 programmable logic controller (PLC) that is responsible for controlling various components in the hydraulic system, testing platform data acquisition, internal joint control, and the dynamometer.

For the hydraulic system (1), the control system includes components such as the oil pump motor, cooling device, proportional pressure regulator, and pressure transmitter. These components are controlled and monitored by the PLC to maintain the desired hydraulic pressure and ensure efficient operation.

In the testing platform data acquisition (2), the control system incorporates strain gauges, encoders, and displacement sensors. These sensors collect data related to the performance and behavior of the system under test. The PLC interfaces with these sensors to acquire and process the data for analysis and monitoring purposes.

The internal joint control (3) involves the use of optical sensors, encoders, and S120 drive units with servo motors. These components enable precise control and positioning of the joints within the system. The PLC receives feedback from the sensors and adjusts the motor control signals accordingly to achieve the desired joint movements.

$$p\left(\theta, \tau^2 \mid \mathbf{y}\right) \propto p\left(\mathbf{y} \mid \mathbf{X}, \theta, \tau^2\right) p(\theta) p\left(\tau^2\right) \tag{20a}$$

$$\propto \prod_{i=1}^{N} \mathcal{N}\left(y_i \mid \mathbf{x}_i^T \theta, \tau^{-2}\right) \prod_{j=1}^{5} \mathcal{N}\left(\theta_j \mid 0, 1\right) \cdot \text{Inv-Gamma}\left(\tau^2 \mid 2, 2\right) \tag{20b}$$

$$\propto \tau^N \exp\left(-\frac{\tau^2}{2} \sum_{i=1}^{N} \left(y_i - \mathbf{x}_i^T \theta\right)^2\right) \prod_{j=1}^{5} \exp\left(-\frac{1}{2}\theta_j^2\right) \cdot \frac{1}{\left(\tau^2\right)^{2+1}} \exp\left(-\frac{2}{\tau^2}\right) \tag{20c}$$

$$\propto \tau^N \exp\left(-\frac{\tau^2}{2} \sum_{i=1}^{N} \left(y_i - \mathbf{x}_i^T \theta\right)^2 - \frac{1}{2} \sum_{j=1}^{5} \theta_j^2 - 2 \cdot \frac{1}{\tau^2}\right) \tag{20d}$$

$$\prod_{i=1}^{N} \mathcal{N}\left(y_i \mid \mathbf{x}_i^T \theta, \tau^{-2}\right) = \mathcal{N}\left(y_1 \mid \mathbf{x}_1^T \theta, \tau^{-2}\right) \times \mathcal{N}\left(y_2 \mid \mathbf{x}_2^T \theta, \tau^{-2}\right) \times \cdots \times \mathcal{N}\left(y_N \mid \mathbf{x}_N^T \theta, \tau^{-2}\right) \tag{21a}$$

$$= \frac{1}{\sqrt{2\pi}\tau^{-1}} \exp\left(-\frac{1}{2} \frac{\left(y_1 - \mathbf{x}_1^T \theta\right)^2}{\tau^{-2}}\right) \times \frac{1}{\sqrt{2\pi}\tau^{-1}} \exp\left(-\frac{1}{2} \frac{\left(y_2 - \mathbf{x}_2^T \theta\right)^2}{\tau^{-2}}\right) \times \cdots \times \frac{1}{\sqrt{2\pi}\tau^{-1}} \exp\left(-\frac{1}{2} \frac{\left(y_N - \mathbf{x}_N^T \theta\right)^2}{\tau^{-2}}\right) \tag{21b}$$

$$= \frac{1}{\left(2\pi\tau^{-2}\right)^{N/2}} \exp\left(-\frac{\tau^2}{2} \sum_{i=1}^{N} \left(y_i - \mathbf{x}_i^T \theta\right)^2\right) \tag{21c}$$

$$= \tau^N \frac{1}{(2\pi)^{N/2}} \exp\left(-\frac{\tau^2}{2} \sum_{i=1}^{N} \left(y_i - \mathbf{x}_i^T \theta\right)^2\right) \tag{21d}$$

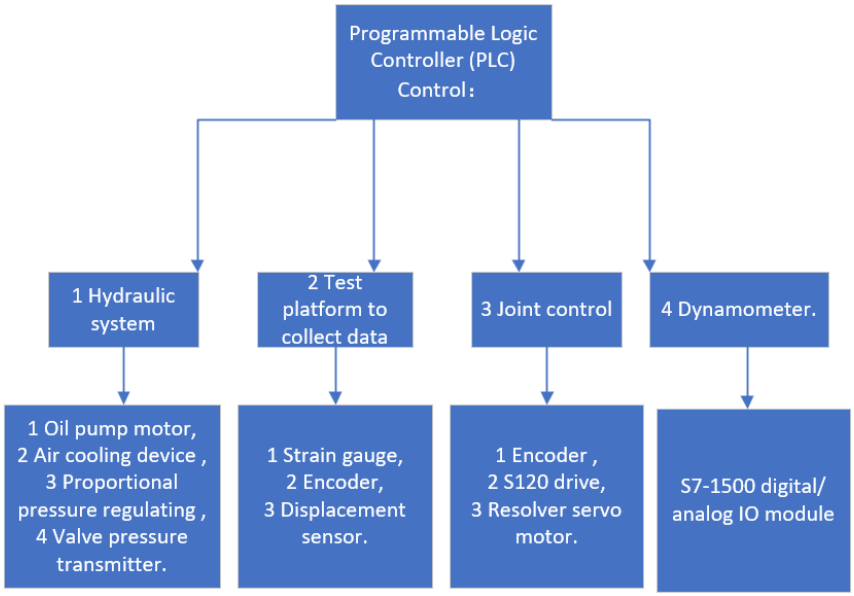

FIGURE 25. Diagram of the control system design of the CMOR fourth joint test platform.

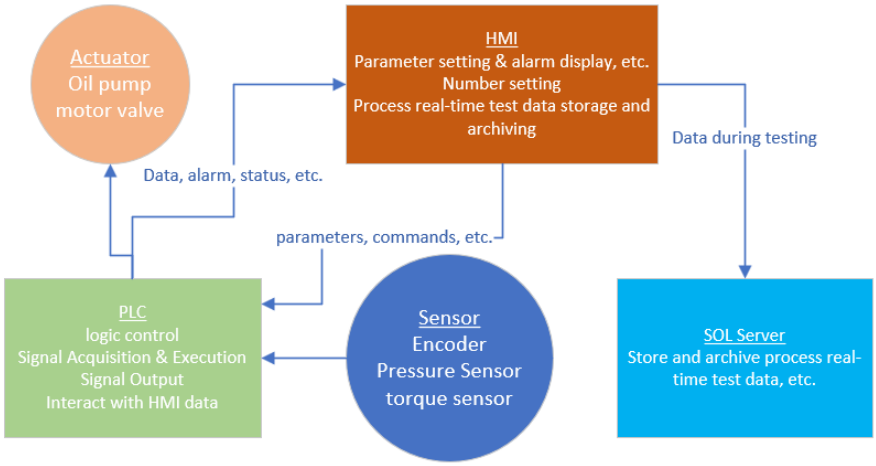

FIGURE 26. The system control scheme which consists of five functional components: sensors, actuators, PLC, HMI, and SQL Server.

Lastly, for the dynamometer (4), the control system includes an S7-1500 digital/analog I/O module. This module allows the PLC to interface with the dynamometer for control and measurement purposes, enabling the assessment of torque and power output.

Overall, the control system integrates the PLC with various sensors, actuators, and modules to monitor and control the different aspects of the hydraulic system, data acquisition, joint control, and dynamometer. This comprehensive control system ensures accurate and reliable operation of the overall system.

The system control scheme in Fig. 26 which consists of five functional components: sensors, actuators, PLC, HMI, and SQL Server. The PLC controls the hydraulic cylinder, allowing for adjustable force output and simulating personalized combinations of shear force and bending moment to achieve various load testing scenarios. The HMI in the control system reads data from sensors, such as the force magnitude of the hydraulic cylinder, and displays and archives this data for further analysis. The SQL Server receives data from the HMI during the testing process and performs analysis tasks, including graphical data visualization, average value analysis, variance analysis, and generation of test platform reports. These reports are then outputted and archived for future reference. By integrating sensors, actuators, PLC, HMI, and SQL Server, the system control solution enables precise control of the hydraulic cylinder, data acquisition from sensors, data visualization and analysis, and report generation for the

testing platform. This comprehensive solution ensures efficient and effective control, monitoring, and analysis of the system.

ACKNOWLEDGMENT

The authors would like to thank them for working overtime to help them run the manipulator. The experiments of this research were conducted in the Wuxi Research Institute, Huazhong University of Science and Technology, Wuxi, Jiangsu, China. The experiment was completed with the assistance of Engineer Cheng and Dr. Hao Zhong.

REFERENCES

[1] L. Sciavicco, B. Siciliano, and L. Villani, "Lagrange and Newton–Euler dynamic modeling of a gear-driven robot manipulator with inclusion of motor inertia effects," *Adv. Robot.*, vol. 10, no. 3, pp. 317–334, Jan. 1995.

[2] M. Makarov, M. Grossard, P. Rodriguez-Ayerbe, and D. Dumur, "Modeling and preview H_∞ control design for motion control of elastic-joint robots with uncertainties," *IEEE Trans. Ind. Electron.*, vol. 63, no. 10, pp. 6429–6438, Oct. 2016.

[3] Y. Qian, S. Han, G. Aguirre-Ollinger, C. Fu, and H. Yu, "Design, modelling, and control of a reconfigurable rotary series elastic actuator with nonlinear stiffness for assistive robots," 2022, *arXiv:2205.14412*.

[4] H. D. Taghirad and P. R. Be'langer, "Modeling and parameter identification of harmonic drive systems," *J. Dyn. Syst., Meas., Control*, vol. 120, no. 4, pp. 439–444, Dec. 1998, doi: 10.1115/1.2801484.

[5] R. Reinhart, Z. Shareef, and J. Steil, "Hybrid analytical and data-driven modeling for feed-forward robot control," *Sensors*, vol. 17, no. 2, p. 311, Feb. 2017.

[6] Z.-S. Hou and Z. Wang, "From model-based control to data-driven control: Survey, classification and perspective," *Inf. Sci.*, vol. 235, pp. 3–35, Jun. 2013.

[7] K. Guo, Y. Pan, and H. Yu, "Composite learning robot control with friction compensation: A neural network-based approach," *IEEE Trans. Ind. Electron.*, vol. 66, no. 10, pp. 7841–7851, Oct. 2019.

[8] X. You, Y. Zhang, X. Chen, X. Liu, Z. Wang, H. Jiang, and X. Chen, "Model-free control for soft manipulators based on reinforcement learning," in *Proc. IEEE/RSJ Int. Conf. Intell. Robots Syst. (IROS)*, Sep. 2017, pp. 2909–2915.

[9] H. Wang, "Adaptive control of robot manipulators with uncertain kinematics and dynamics," *IEEE Trans. Autom. Control*, vol. 62, no. 2, pp. 948–954, Feb. 2017.

[10] C. W. Kennedy and J. P. Desai, "Modeling and control of the Mitsubishi PA-10 robot arm harmonic drive system," *IEEE/ASME Trans. Mechatronics*, vol. 10, no. 3, pp. 263–274, Jun. 2005, doi: 10.1109/TMECH.2005.848290.

[11] H. Zhang, S. Ahmad, and G. Liu, "Torque estimation for robotic joint with harmonic drive transmission based on position measurements," *IEEE Trans. Robot.*, vol. 31, no. 2, pp. 322–330, Apr. 2015.

[12] F. Yu, S. Xiao, M. Zhu, and Z. Wang, "A novel method to improve the accuracy of torque estimation for robotic joint with harmonic drive transmission," *Eng. Lett.*, vol. 26, no. 4, pp. 455–460, Jan. 2018.

[13] Z. Yao, H. Wu, Y. Yang, Y. Cheng, H. Pan, T. Zhang, and R. Yin, "On-line precision control of CFETR multipurpose overload robot using deformation model," *Fusion Eng. Design*, vol. 174, Jan. 2022, Art. no. 112967.

[14] M. Li, H. Wu, H. Handroos, R. Skilton, A. Hekmatmanesh, and A. Loving, "Deformation modeling of manipulators for DEMO using artificial neural networks," *Fusion Eng. Design*, vol. 146, pp. 2401–2406, Sep. 2019.

[15] T. Chen, E. B. Fox, and C. Guestrin, "Stochastic gradient Hamiltonian Monte Carlo," in *Proc. Int. Conf. Mach. Learn. (ICML)*, vol. 32, 2014, pp. 1683–1691.

[16] C.-H. Choi, A. Tesini, R. Subramanian, A. Rolfe, S. Mills, R. Scott, T. Froud, B. Haist, and E. McCarron, "Multi-purpose deployer for ITER in-vessel maintenance," *Fusion Eng. Design*, vols. 98–99, pp. 1448–1452, Oct. 2015.

[17] T. Zhang, Y. Shi, Y. Cheng, Y. Zeng, X. Zhang, and S. Liang, "The design and implementation of distributed architecture in the CMOR motion control system," *Fusion Eng. Design*, vol. 186, Jan. 2023, Art. no. 113357.

[18] S. P. Brooks, A. Gelman, G. L. Jones, and X.-L. Meng, *Handbook of Markov Chain Monte Carlo*. London, U.K.: Chapman & Hall, 2011.

[19] J. Sarkis and D. G. Dhavale, "Supplier selection for sustainable operations: A triple-bottom-line approach using a Bayesian framework," *Int. J. Prod. Econ.*, vol. 166, pp. 177–191, Aug. 2015.

[20] E. Thrane and C. Talbot, "An introduction to Bayesian inference in gravitational-wave astronomy: Parameter estimation, model selection, and hierarchical models," *Publications Astronomical Soc. Aust.*, vol. 36, pp. 1–12, Mar. 2019.

[21] O. Ryan, M. Zondervan-Zwijnenburg, S. Depaoli, R. van de Schoot, and S. D. Winter, "A systematic review of Bayesian articles in psychology: The last 25 years," *Psychol. Methods*, vol. 22, no. 2, pp. 217–239, Jun. 2017.

[22] J. Hendriks, A. Wills, B. Ninness, and J. Dahlin, "Practical Bayesian system identification using Hamiltonian Monte Carlo," 2020, *arXiv:2011.04117*.

[23] I. Murray, R. P. Adams, and D. Mackay, "Elliptical slice sampling," in *Proc. JMLR*, 2010, pp. 541–548.

[24] R. Nishihara, I. Murray, and R. P. Adams, "Parallel MCMC with generalized elliptical slice sampling," *J. Mach. Learn. Res.*, vol. 15, no. 1, pp. 2087–2112, 2014.

[25] R. M. Neal, "MCMC using Hamiltonian dynamics," 2012, *arXiv:1206.1901*.

[26] M. Welling and Y. W. Teh, "Bayesian learning via stochastic gradient Langevin dynamics," in *Proc. 28th Int. Conf. Mach. Learn.*, 2011, pp. 1–8.

[27] T. Radivojević and E. Akhmatskaya, "Modified Hamiltonian Monte Carlo for Bayesian inference," *Statist. Comput.*, vol. 30, no. 2, pp. 377–404, Mar. 2020.

[28] L. Hao, R. Pagani, M. Beschi, and G. Legnani, "Dynamic and friction parameters of an industrial robot: Identification, comparison and repetitiveness analysis," *Robotics*, vol. 10, no. 1, p. 49, Mar. 2021. [Online]. Available: https://www.mdpi.com/2218-6581/10/1/49

[29] Q. Wang, H. Wu, Y. Cheng, H. Pan, Y. Yang, and G. Qin, "Friction-identification of harmonic drive joints based on the MCMC method," *IEEE Access*, vol. 10, pp. 125893–125907, 2022, doi: 10.1109/ACCESS.2022.3226036.

[30] M. Ruderman, F. Hoffmann, and T. Bertram, "Modeling and identification of elastic robot joints with hysteresis and backlash," *IEEE Trans. Ind. Electron.*, vol. 56, no. 10, pp. 3840–3847, Oct. 2009, doi: 10.1109/tie.2009.2015752.

[31] J. Cai, W. Dong, and R. Nagamune, "A survey of Bouc–Wen hysteretic models applied to piezo-actuated mechanical systems: Modeling, identification, and control," *J. Intell. Mater. Syst. Struct.*, vol. 34, Mar. 2023, Art. no. 1045389X2311573, doi: 10.1177/1045389x231157361.

[32] C.-X. Li, L.-L. Li, G.-Y. Gu, and L.-M. Zhu, "Modeling of rate-dependent hysteresis in piezoelectric actuators using a Hammerstein-like structure with a modified Bouc–Wen model," in *Proc. 9th Int. Conf. Intell. Robot. Appl. (ICIRA)*. Tokyo, Japan: Springer, 2016, pp. 672–684.

[33] S. Kang, H. Wu, Y. Li, X. Yang, and J. Yao, "A fractional-order normalized Bouc–Wen model for piezoelectric hysteresis nonlinearity," *IEEE/ASME Trans. Mechatronics*, vol. 27, no. 1, pp. 126–136, Feb. 2022.

[34] G. Qin, A. Ji, Y. Cheng, W. Zhao, H. Pan, S. Shi, and Y. Song, "Position error compensation of the multi-purpose overload robot in nuclear power plants," *Nucl. Eng. Technol.*, vol. 53, no. 8, pp. 2708–2715, Aug. 2021.

[35] S. K. Dwivedy and P. Eberhard, "Dynamic analysis of flexible manipulators, a literature review," *Mechanism Mach. Theory*, vol. 41, no. 7, pp. 749–777, Jul. 2006.

[36] M. Ruderman, T. Bertram, and M. Iwasaki, "Modeling, observation, and control of hysteresis torsion in elastic robot joints," *Mechatronics*, vol. 24, no. 5, pp. 407–415, Aug. 2014.

[37] F. Ikhouane and J. Rodellar, *Systems with Hysteresis: Analysis, Identification and Control Using the Bouc–Wen Model*. Hoboken, NJ, USA: Wiley, 2007.

[38] M. Gautier, "Identification of robots dynamics," *IFAC Proc. Volumes*, vol. 19, no. 14, pp. 125–130, Dec. 1986.

[39] J. Swevers, "Dynamic model identification for industrial robots," *IEEE Control Syst. Mag.*, vol. 27, no. 5, pp. 58–71, Oct. 2007, doi: 10.1109/MCS.2007.904659.

[40] P.-R. Loh, G. Tucker, B. K. Bulik-Sullivan, B. J. Vilhjálmsson, H. K. Finucane, R. M. Salem, D. I. Chasman, P. M. Ridker, B. M. Neale, B. Berger, N. Patterson, and A. L. Price, "Efficient Bayesian mixed-model analysis increases association power in large cohorts," *Nature Genet.*, vol. 47, no. 3, pp. 284–290, Mar. 2015.

[41] D. P. Kingma and M. Welling, "Auto-encoding variational Bayes," 2013, *arXiv:1312.6114*.

[42] M. D. Hoffman and A. Gelman, "The No-U-Turn Sampler: Adaptively setting path lengths in Hamiltonian Monte Carlo," *J. Mach. Learn. Res.*, vol. 15, no. 1, pp. 1593–1623, 2014.
[43] J. S. Liu and J. S. Liu, *Monte Carlo Strategies in Scientific Computing*, vol. 75. New York, NY, USA: Springer, 2001.
[44] M. Betancourt, "A conceptual introduction to Hamiltonian Monte Carlo," 2017, *arXiv:1701.02434*.
[45] R. M. Neal, *Bayesian Learning for Neural Networks*, vol. 118. New York, NY, USA: Springer, 2012.
[46] X. Zhu, X. Lu, and C. Xu, "Research on parameter identification of mild steel damper based on Bouc–Wen model," (in Chinese), *Struct. Eng.*, vol. 27, no. 5, pp. 124–128, 2011.
[47] A. W. Smyth, S. F. Masri, A. G. Chassiakos, and T. K. Caughey, "On-line parametric identification of MDOF nonlinear hysteretic systems," *J. Eng. Mech.*, vol. 125, no. 2, pp. 133–142, Feb. 1999.
[48] D. Foreman-Mackey, D. W. Hogg, D. Lang, and J. Goodman, "emcee: The MCMC hammer," *Publications Astronomical Soc. Pacific*, vol. 125, no. 925, pp. 306–312, Mar. 2013.
[49] D. Vats and C. Knudson, "Revisiting the Gelman–Rubin diagnostic," *Stat. Sci.*, vol. 36, no. 4, pp. 518–529, Nov. 2021.
[50] M. Sobol, "On sensitivity estimation for nonlinear mathematical models," *Matematicheskoe Modelirovanie*, vol. 2, no. 1, pp. 112–118, 1990.
[51] T. Homma and A. Saltelli, "Importance measures in global sensitivity analysis of nonlinear models," *Rel. Eng. Syst. Saf.*, vol. 52, no. 1, pp. 1–17, Apr. 1996.
[52] A. Gelman, J. B. Carlin, H. S. Stern, and D. B. Rubin, *Bayesian Data Analysis*. London, U.K.: Chapman & Hall, 1995.

QI WANG received the M.S. degree in mechanical systems from the University of Technology de Troyes, Troyes, France, in 2015. She is currently pursuing the Ph.D. degree with the Lappeenranta University of Technology, Finland. She is also concurrently a Mechanical Engineer with the Institute of Plasma Physics, Hefei Institutes of Physical Science, Chinese Academy of Sciences (ASIPP), Hefei, China. Her primary research interests include parameter identification and dynamic control of robots.

HUAPENG WU holds the position of a Docent and a Doctoral Tutor with the Lappeenranta University of Technology, Finland. Additionally, he plays a crucial role as a representative of the European Union in fostering nuclear fusion cooperation between China and Europe. With extensive experience in the field, he has devoted significant efforts to the development of remote-control robots for nuclear fusion reactors. Throughout his career, he has achieved remarkable milestones in industrial robotics research and has been credited with over 50 significant academic publications.

YUNTAO SONG received the D.Sc. (Tech.) degree from the Institute of Plasma Physics, Chinese Academy of Sciences (ASIPP), Hefei, China, in 2001. For the past 12 years, he has been dedicated to magnetic confinement fusion system engineering research. He is actively involved in research concerning the application of robotics technology in remote handling to enhance the safety and automation of fusion reactors and the design of a novel proton therapy systems. He holding the position of a Full Professor with ASIPP and USTC and he continues to make significant advancements in his research endeavors.

HEIKKI HANDROOS (Member, IEEE) received the M.Sc. (Eng.) and D.Sc. (Tech.) degrees from Tampere University, Finland, in 1985 and 1991, respectively. He has been a Full Professor in machine automation with LUT University, since 1992. He has published more than 300 journals and conference papers in the field of mechatronics, robotics, and control. He has been the supervisor of about 30 doctoral students. He has served as a principal investigator of international and domestic projects, whose total funding exceeds 30M. He is a member of ASME. He has served as an Associate Editor for the *ASME Journal of Dynamic Systems, Measurement, and Control*, from 2013 to 2020.

YONG CHENG received the M.S. degree from the Hefei University of Technology. He is currently pursuing the Ph.D. degree with the University of Science and Technology of China. He is also the Deputy Director of the Tokamak Design Division, Institute of Plasma Physics, Chinese Academy of Sciences. With extensive experience in remote-control robot development for nuclear fusion reactors, he has dedicated significant time to this field. His research interest includes remote handling robotics, furthering advancements in this area.

GUODONG QIN received the M.S. degree in mechanical and electronic engineering from the Anhui University of Technology, China, in 2018, and the joint Ph.D. degree from the School of Mechanical Engineering, Nanjing University of Aeronautics and Astronautics, and the Lappeenranta University of Technology. His research interests include remote-handling robot structure design and motion planning.